The late Holocene Nealtican lava-flow field, Popocatépetl volcano, central Mexico: Emplacement dynamics and future hazards

Israel Ramírez-Uribe, Claus Siebe, Oryaëlle Chevrel, Dolors Ferres, Sergio Salinas

The late Holocene Nealtican lava-flow field, Popocatépetl volcano, central Mexico: Emplacement dynamics and future hazards

Israel Ramírez-Uribe[1,†], Claus Siebe[1], Magdalena Oryaëlle Chevrel[2], Dolors Ferres[3], and Sergio Salinas[4]

[1]*Departamento de Vulcanología, Instituto de Geofísica, Universidad Nacional Autónoma de México, Coyoacán, C.P. 04510, Ciudad de México, Mexico*

[2]*Université Clermont Auvergne, CNRS, IRD, OPGC, Laboratoire Magmas et Volcans, F-63000 Clermont-Ferrand, France*

[3]*Escuela Nacional de Ciencias de la Tierra, Universidad Nacional Autónoma de México, Coyoacán, C.P 04510, Ciudad de México, Mexico*

[4]*División de Ingeniería en Ciencias de la Tierra, Facultad de Ingeniería, Universidad Nacional Autónoma de México, Coyoacán, C.P. 04510, Ciudad de México, Mexico*

ABSTRACT

Popocatépetl, one of the most hazardous volcanoes worldwide, poses significant threats for nearby populations in central Mexico. Therefore, it is important to reconstruct its eruptive history, including estimates of lava-flow emplacement times and their rheological properties. These studies define possible future eruptive scenarios and are necessary to mitigate the risk. Stratigraphic studies of the cal 350–50 B.C. Lorenzo Plinian pumice sequence indicate that effusive activity (Nealtican lava-flow field) occurred shortly after explosive activity, reflecting drastic changes in the eruptive dynamics. It was likely due to the efficient degassing of the magma during the Plinian phase and a decrease of magma ascent and decompression rates. Magma mixing, fractional crystallization, and a minor crust assimilation are the processes controlling the differentiation of the Nealtican lavas. We used lava chemical and mineralogical composition to estimate lava-flow viscosities, and used high-resolution elevation data to estimate emplacement times. Results indicate that lava viscosities of andesites and dacites ranged from 10^9 to 10^{12} Pa·s and emplacement durations were between ~1 and ~29 years, depending on the flow unit and morphological method employed. Considering the entire volume of emitted lava (4.2 km^3) and a mean output rate of ~1 m^3/s to ~15 m^3/s, we estimated that the effusive phase that produced the Nealtican lava-flow field may have lasted ~35 years. This eruption had a considerable impact on pre-Hispanic settlements around the volcano, whose population exodus and relocation probably contributed to the rise of important cities in central Mexico, such as Teotihuacán and Cholula.

INTRODUCTION

Popocatépetl is a polygenetic volcano of andesitic-dacitic composition (Robin, 1984; Schaaf et al., 2005) in the east-central part of the Trans Mexican volcanic belt (TMVB) (Fig. 1). It is considered one of Mexico's and the world's potentially most dangerous volcanoes owing to the high-magnitude explosive eruptions documented in its late Pleistocene-Holocene stratigraphic record (e.g., Siebe et al., 1996a, 2017; Espinasa-Pereña and Martín Del Pozzo, 2006; Arana-Salinas et al., 2010; Sosa-Ceballos et al., 2012) and the high population density of the region (Siebe and Macías, 2004). After several decades of quiescence, a gradual increase in seismic and fumarolic unrest was noticed from 1993 until the volcano reawakened on December 21, 1994 (De la Cruz-Reyna and Siebe, 1997). Since then, it has experienced almost continuous fumarolic activity (e.g., Goff et al., 1998; Love et al., 1998; Stremme et al., 2011; Campion et al., 2018; Taquet et al., 2019) and recurrent effusive and explosive eruptions associated with the growth and destruction of >70 lava domes inside its crater (Sheridan et al., 2001; Macías and Siebe, 2005; Espinasa-Pereña, 2012; Gómez-Vazquez et al., 2016; Mendoza-Rosas et al., 2017; Macías et al., 2020). Many of these studies have been used in the preparation of volcano hazard maps such as that of Macías et al. (1995) and its latest update, which includes a technical report prepared by a large team (Martin-Del Pozzo et al., 2017).

Although a large portion of its products stem from explosive pyroclastic eruptions, numerous lava flow fields attest to the importance of effusive activity. One of the largest in volume and area covered is the Nealtican lava flow field, locally known as "Pedregal de Nealtican" (pedregal = rocky area in Spanish) on the eastern flank of the edifice (Fig. 1).

Previous studies suggest that the petrological and geochemical diversity of products found at some Mexican volcanoes reflects mixing between different magmatic components, whose residence in long-lived magma chambers can eventually lead to an effective homogenization (Nelson, 1980; Luhr and Carmichael, 1982; Nixon, 1988a, 1988b; Robin et al., 1991; Gómez-Tuena et al., 2005). Various studies have invoked pre-eruptive mixing of mafic and evolved magmas in the formation of Popocatépetl's products (e.g., Straub and Martin Del Pozzo, 2001; Witter et al., 2005; Schaaf et al., 2005; Atlas et al., 2006; Arana-Salinas et al., 2010; Sosa-Ceballos et al., 2014, 2015; Siebe et al., 2017; Mangler et al., 2019). Thus, Sosa-Ceballos et al. (2014) argued that magma mixing has occurred shortly before Plinian eruptions during at least the past ~23,000 years.

Here we focus on the Nealtican lava-flow field that covers a large part of the eastern flank of Popocatépetl volcano in the Mexican state of Puebla (Fig. 1). This flow field was formed shortly after the emplacement of the Lorenzo Plinian pumice sequence radiocarbon-dated at ~2150 yr B.P. (range ± 2σ, cal 350–50 B.C.) (Siebe et al., 1996a; Panfil et al., 1999), reflecting drastic changes in the eruptive dynamics. Recent availability of high-resolution elevation data allowed us to precisely map the lava flow units, determine their volumes, highlight their

†isramirez.u@gmail.com.

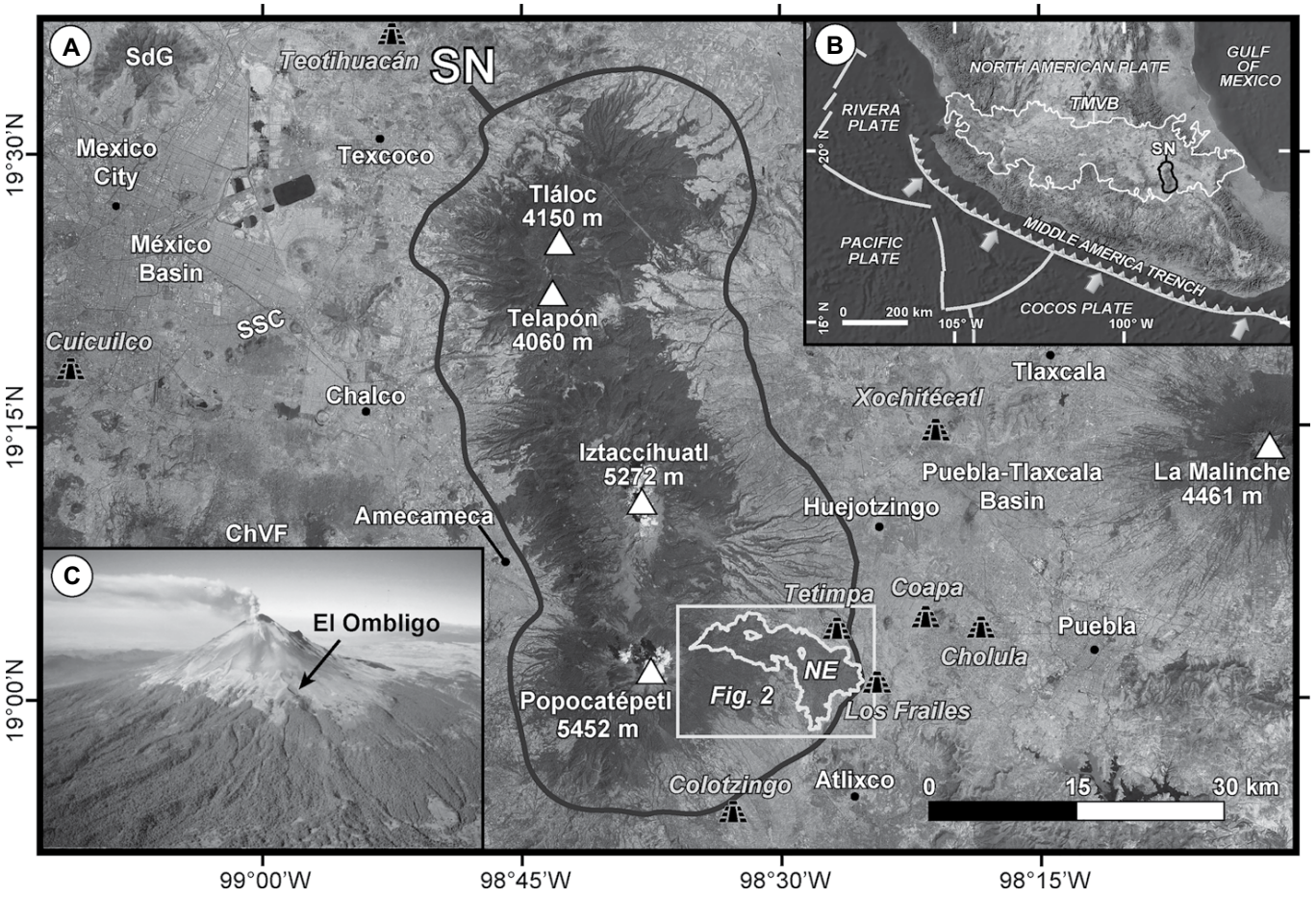

Figure 1. Index maps. (A) Satellite image (Microsoft® Bing Maps, 2019) of the Sierra Nevada (SN, outlined in black) showing the location of the Popocatépetl volcano study area (white rectangle denotes area covered in Figure 2 showing the Nealtican lava-flow field), adjacent basins, and major cities. NE—Nealtican lava-flow field. White triangles indicate volcanoes mentioned in the text. Other volcanic landforms are ChVF—Chichinautzin Volcanic Field, SdG—Sierra de Guadalupe, and SSC—Sierra de Santa Catarina. Black pyramids indicate archaeological sites mentioned in the text. Inset map (B) location of the SN within the Trans Mexican volcanic belt (TMVB) and major plate-tectonic features of southern Mexico. Inset aerial photo (C) Popocatépetl volcano from the NE (taken December 1994, courtesy of John Ewert) and the El Ombligo alignment of vents from which the Nealtican lava-flow field emanated.

main morphological features in detail, and measure their physical parameters. This offered the opportunity to apply morphology-based methods to estimate flow emplacement durations and eruption rates. Chemical and petrological analyses of different lava units were used to constrain the magma sources, pre-eruptive storage conditions, and lava rheology.

BACKGROUND

Geological Context

The TMVB is a continental volcanic arc constituted by ~8000 volcanic structures (Demant, 1978; Gómez-Tuena et al., 2005), which is tectonically related to the subduction of the oceanic Cocos and Rivera plates underneath the North American continental plate along the Mesoamerican trench (Fig. 1A; Nixon, 1982; Pardo and Suárez, 1995; Gómez-Tuena et al., 2005). The Popocatépetl volcano (5452 m above sea level) is located 65 km southeast of Mexico City (~25 million inhabitants) and 40 km west of the city of Puebla (~7 million inhabitants). The volcano forms the southernmost and youngest edifice of the N-S–trending, 80-km-long Sierra Nevada volcanic range, which includes the Iztaccíhuatl, Tláloc, and Telapón volcanoes (Cadoux et al., 2011; Macías et al., 2012) to the north (Fig. 1). This range separates the Mexico Basin to the west from the Puebla-Tlaxcala Basin to the east. The isotopic ages ($^{40}Ar/^{39}Ar$) of rocks forming the Sierra Nevada (Tláloc, Telapón, Iztaccíhuatl, and Popocatépetl volcanoes) range from 1.8 Ma to the present (Cadoux et al., 2011; García-Tovar and Martínez-Serrano, 2011; Macías et al., 2012). Popocatépetl's complex evolution included at least four stages of cone construction and destruction (Siebe et al., 1995, 2017; Sosa-Ceballos et al., 2012, 2015; Martin-Del Pozzo et al., 2017).

Popocatépetl's stratigraphic record for the last 23,000 years includes at least six major Plinian eruptions (Siebe et al., 2017). More recent Plinian eruptions include the cal 3945–3640 B.C. "Ochre pumice" (Arana-Salinas et al., 2010), the cal 350–50 B.C. "Lorenzo pumice," and the cal A.D. 680–970 "Pink Pumice" eruptions (Siebe et al., 1996a; Panfil et al., 1999). All calibrated age-ranges are at the 2σ level using the software CALIB 8.2 developed by Stuiver et al. (2021). These last three eruptions occurred within the time of human occupation. Especially the last

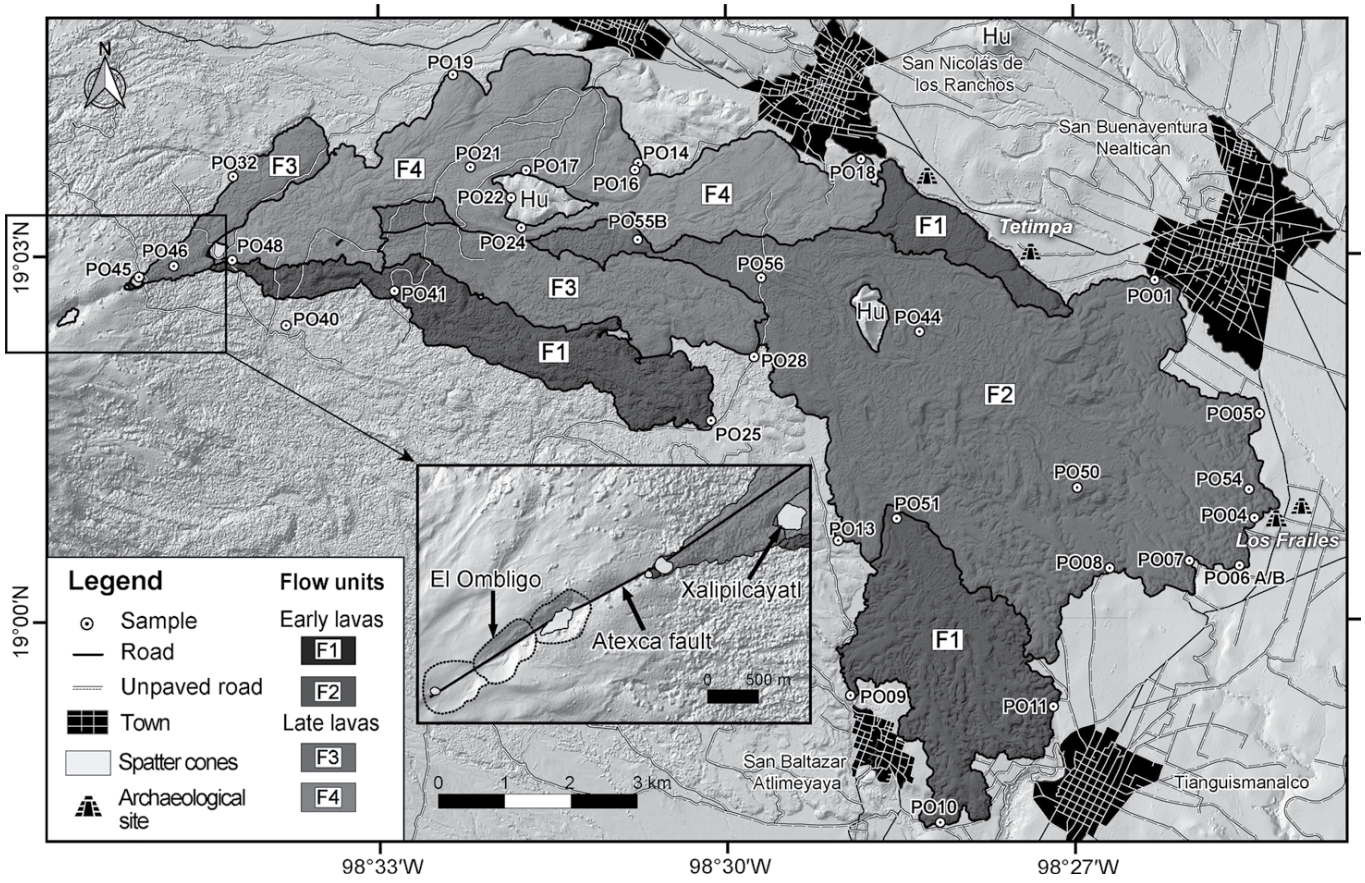

Figure 2. Hillshade-Digital Elevation Model (DEM) of the Nealtican lava flow field of the Popocatépetl volcano showing the emplacement sequence of its different flow units (F1 to F4). Inset shows the NE-SW El Ombligo-Xalipilcáyatl emission fissure. Rock-sampling points, archaeological sites, hummocks (Hu) from an older debris avalanche deposit from the Iztaccíhuatl volcano, and towns are also indicated.

two affected pre-Hispanic settlements in the region, as attested to by several archaeological sites. As first documented by Seele (1973) at the Tetimpa and Los Frailes sites (Fig. 2), pyroclastic flow, pumice fallout, and lahar deposits, as well as the Nealtican lava flows buried numerous archaeological remains (Siebe et al., 1996a; Plunket and Uruñuela, 2005). The last two Plinian eruptions of Popocatépetl roughly coincide with important transitions in Mesoamerican history: The "Lorenzo pumice" eruption dated at cal 350–50 B.C. falls within the pre-Classic to Classic transition while the cal A.D. 680–970 "Pink pumice" eruption coincides with the transition from the Classic to the post-Classic periods (Siebe et al., 1996a).

Popocatépetl and its ~0.8 km diameter summit crater formed mainly above a central conduit system that has fed numerous Plinian eruptions, but also domes and lava flows (Siebe et al., 1996b). Subordinate lateral upper-flank vents (Fig. 2) are aligned along the NE-SW Atexca fault (Martin-Del Pozzo et al., 2017; Arámbula-Mendoza et al., 2010). On the NE flank of the cone and along this fault, activity was most intense in the El Ombligo area (Figs. 1B and 2).

The local basement cropping out around Popocatépetl, first described by Fries (1960, 1966), consists of Cretaceous marine limestone (Cuautla and Morelos formations) folded during the Laramide orogeny and discordantly covered by terrestrial sediment of the Eocene-Oligocene Balsas Group. These were intruded by granodiorite that generated contact aureoles forming skarn-type mineral deposits (Aguilar-Murillo, 2012; Mares-Tepanohaya, 2014). Volcanism in the area probably started in the Miocene, evidenced by the calc-alkaline rocks of the Tepexco Formation (Fries, 1960).

Lava Flows

The lava-flow dynamic depends on several factors including eruption rate, underlying topography, and its rheology, which control the advance rate and the behavior of lava flows (Griffiths, 2000). Such factors have been closely studied on active basaltic lava flows. The evolution of lava-flow features and physical properties as a function of cooling rate during emplacement are now used for modeling trajectories and advances of active flows (e.g., recent basaltic eruptions of Etna (Sicily, Italy), Kilauea (Hawaii, USA), and Piton de la Fournaise (Réunion, France) volcanoes; Wright et al., 2008; Vicari et al., 2011; Harris et al., 2019). Silicic andesite and dacite flows have rarely been witnessed (e.g., eruptions of dacitic block flow at Santiaguito volcano, Guatemala, and andesitic lava flow at Sinabung volcano, Indonesia; Harris et al., 2002; Carr et al., 2019), and their dynamics remain an important research topic.

Currently, instruments to directly measure active lava flow viscosities greater than 10^5 Pa·s (typical for evolved compositions such as andesites, dacites, and rhyolites) are not available and viscosity measurements in the field remain a great challenge (Chevrel et al., 2019). Until more reliable data on active silicic flows becomes available, the connections between the characteristics preserved in solidified lavas and flow dynamics can provide insight to understand

the behavior of a flow (e.g., Chevrel et al., 2013; Robert et al., 2014; Latutrie et al., 2017).

Flow geometry, structure, and surface morphology offer hints about eruption rates and lava rheology (Hulme and Fielder, 1977; Griffiths, 2000). Rheological models have been developed to estimate the apparent viscosity of lava flows by their dimensions (e.g., Nichols, 1939; Hulme, 1974; Griffiths and Fink, 1993; Pinkerton and Wilson, 1994; Kerr and Lyman, 2007; Castruccio et al., 2013). In recent years, high-resolution digital elevation models have been used successfully for these purposes (e.g., Dietterich et al., 2018; Younger et al., 2019; Ramírez-Uribe et al., 2021; Reyes-Guzmán et al., 2021).

The present work takes advantage of the recent acquisition of high-resolution elevation data and the geological youthfulness of the lava flows. Together these allow the flow emplacement parameters of the Nealtican lava-flow field from the Popocatépetl volcano to be constrained.

METHODS AND DATA SETS

Mapping and Lava Volume Estimates

During 2015, several campaigns were undertaken, in which the entire perimeter of the Nealtican lava-flow field was covered. A total of 32 lava samples were collected, both from lava fronts and inside the units. In the field, we identified the contact of lavas with the deposits of the Lorenzo Plinian pumice. We also collected 10 Lorenzo pumice samples (PO40-LP-A to PO40-LP-J) in a ~7-m-deep trench ~4 km to the east of the main crater (Table S1, Supplemental Material 1[1]).

A geological map was elaborated from the Nealtican lava-flow field area using topographic charts, digital elevation models (DEMs) with a resolution of 3 and 5 m from INEGI (Instituto Nacional de Estadística, Geografía e Informática, Mexico), and Google Earth (2002–2018) satellite images. This map was developed using QGIS software. The DEMs were obtained by INEGI with a correlation method of satellite images by applying photogrammetric processes. The different lava-flow units were delimited and color-coded to indicate their chronological emplacement order (Fig. 2). This was accomplished by analyzing their morphology, comparing their chemical compositions, and field observations. Accordingly, we defined four major flow units (F1–F4), where units F1 and F2 are clearly stratigraphically below units F3 and F4, forming the early and late lava groups, respectively.

For lava volumes we extracted the contour lines from the 5 m resolution DEM, and clipped out the area covered by a polygon delimiting the Nealtican lava-flow field. The topographic relief before the emplacement of the lava-flow field was reconstructed by interpolating the 5 m topographic lines. For this, we drew in QGIS their most probable continuation using the surrounding topographic line patterns as a guide (methodology described in Chevrel et al., 2016a and Larrea et al., 2017), and obtained an irregular topography beneath the present lava flows. The topographic lines were "reconstructed" considering the principle of continuity to the nearest contour line and the average thickness for lava flows. The surface below the lavas was obtained interpolating the new generated curves with a triangular irregular network model. The volume of the lava flow field was then estimated by subtracting the interpolated paleo-surface from the actual topography. For simplicity, we drew two lava polygons, one for lava flow units F1–F3 and the other for lava flow unit F4, before applying a mask to extract the volumes of each composition group. However, lava flow unit F3 is transitional in composition, but the sampling of this flow is not sufficient to determine exactly where we can divide the flow into andesite and dacite.

Lava Sample Analysis

Petrography and chemical composition

Petrographic analysis was used to characterize the mineralogical properties and to estimate modes. Modes were determined by point counting, using 1000 points per thin-section. Modal proportions of phenocrysts ($\geq$0.3 mm), microphenocrysts (<0.3–0.15 mm), vesicles, as well as glass were calculated on at least two samples from each flow unit. Microlites (<0.15 mm) were not considered because their proportions were difficult to obtain.

Chemical analyses of major and trace elements (Table S1, Supplemental Material 1) were carried out at Activation Laboratories Ltd. (Actlabs), Ancaster, Canada and analytical methods included fusion–inductively coupled plasma (FUS-ICP), total digestion–-inductively coupled plasma (TD-ICP), and instrumental neutron activation analysis (INAA). For more information about the analytical procedures see the Activation Laboratories Web site (http://www.actlabs.com) and Agustín-Flores et al. (2011).

Additionally, mineral and glass compositions (Table S2, Supplemental Material 2) were determined using an electron microprobe (JEOL JXA-8230 Superprobe) at the Microanalysis Laboratory of the Instituto de Geofísica, Universidad Nacional Autónoma de México, Campus Morelia. Selected thin sections were vacuum carbon-coated and the measuring conditions were an accelerating voltage of 15 kV and a beam current of 10 nA (with a diameter of 1 μm), and counting times were 40 s for Ti, Fe, and Mg, and 10 s for K, Na, Ca, Si, and Al. The beam was focused for mineral phases and defocused to 10 μm for groundmass glass. Element measurements were calibrated from a variety of reference mineral standards, which were: PETL (rutile) for Ti, LIFL (fayalite) for Fe, PETJ (orthoclase) for K, TAP (albite) for Na, PETJ (diopside) for Ca, TAP (orthoclase) for Si, TAP (albite) for Al, and TAP (diopside) for Mg. In addition, backscattered-electron (BSE) images were obtained to observe details of the different mineral phases. Average compositions of glass and minerals in Nealtican lava flow samples are listed in Table S2, Supplemental Material 2.

Thermobarometry

Crystallization temperatures and pressures (Table S3, Supplemental Material 3) were obtained via a series of thermobarometers (Putirka, 2008). We used microprobe data obtained on phenocrysts and micro-phenocrysts: the olivine-liquid geothermometer (Beattie, 1993), the clinopyroxene-liquid geothermobarometer (Putirka et al., 1996, 2003), the orthopyroxene-liquid geothermobarometer (Beattie, 1993), and the plagioclase-liquid geothermometer (Putirka, 2005). Additionally, the Fe-Ti oxide geothermometer (Ghiorso and Evans, 2008) was applied. Note that for geothermometers, only results that passed the equilibrium-tests, as suggested by Putirka (2008), were considered. For the olivine-liquid thermometer we used a pressure value following Witter et al. (2005) and Roberge et al. (2009), who indicate that pressure (estimated from melt inclusions in olivine from Popocatépetl) rarely exceeded 400 MPa. This value is therefore considered as the maximum pressure limit for olivine crystallization. To estimate water contents, we applied the plagioclase-liquid hygrometer of Waters and Lange (2015) by using temperatures previously obtained by the plagioclase-liquid geothermometer and a pressure of 150 MPa (Popocatépetl pressure data from Witter et al., 2005), which are similar to the experimental data for Popocatépetl's plagioclases obtained by Sosa-Ceballos et al. (2014). Details of the methods and equilibrium tests are provided in Supplemental Material 3.

[1]Supplemental Material. Tables S1–S5 and methods for geothermobarometric and hygrometric calculations, and methods for estimating rheological properties of lava flow and their emplacement times. Please visit https://doi.org/10.1130/GSAB.S.18809951 to access the supplemental material, and contact editing@geosociety.org with any questions.

Estimation of Viscosity from Lava Sample Analyses

Lava viscosity was calculated assuming a mixture of melt and crystals based on the petrographic characteristics of the samples. The effect of gas bubbles was not considered since the amounts of vesicles in the analyzed samples are relatively low. The melt phase viscosity is calculated via the model of Giordano et al. (2008) that considers temperature, major-element composition, and H_2O content. The effect of crystals on viscosity was evaluated by considering two populations of crystals simulating angular equant and angular prolate shapes, for mafic and plagioclase crystals, respectively. For this we applied the Costa et al. (2009) equations with the fitting parameters given in Cimarelli et al. (2011). Details of the equations used are given in Supplemental Material 4.

Accordingly, for pre-eruptive conditions, we considered the recalculated chemical composition of the interstitial melt (without phenocrysts), the crystallization temperature obtained from geothermometry, the amount and shape of phenocrysts, and H_2O content obtained from hygrometry. The recalculated interstitial-melt chemical composition was obtained by subtraction of phenocrysts, according to their percentages, from the whole rock composition (Table S4, Supplemental Material 4). For syn-eruptive conditions, we calculated the lava viscosity at the temperatures previously estimated and considered the amount and shape of phenocrysts and micro-phenocrysts we obtained from petrographic analyses and an evolved melt phase. In this case, the melt-phase viscosity was calculated using the glass compositions (interstitial liquid) from microprobe data and by assuming a low dissolved water content (0.1 wt% H_2O) due to gas-exsolution at the moment of eruption.

Eruption Rates and Flow Duration

Lava flow dimensions and morphologies can be used to estimate eruption rates, velocities, and emplacement-duration time scales. Flow dimensions (length, width, and thickness) were extracted from the best exposed lavas (units F3 and F4) using the 3-m-resolution DEM (Fig. 3). This data was used for the volume estimation of individual flows (units F3 and F4). In the case of F4 we used a simplified area of the flow unit for obtaining the morphological parameters (see Fig. 3). The average flow width and thickness were derived from nine profiles perpendicular to the flow direction (Fig. 3), and we identified some channels and levees (Fig. 4). Each profile is an average of five individual measurements spaced one meter apart. The total flow length represents an average of five vent-front measurements. The topographic gradient was inferred adjacent to the lava flow where the underlying topography is exposed as well as on the flow surface by using the reconstructed pre-eruptive topography we created.

A common method considers that the whole flow behaves as a laminar Newtonian fluid (neglecting post-emplacement inflation or deflation; Harris and Rowland, 2015) and the average flow velocity is calculated via the Jeffreys (1925) equation. For this we considered an average flow thickness and the mean lava viscosity obtained from the sample's petrological analyses at syn-eruptive conditions (Table S5, Supplemental Material 4). The velocity was then converted to an eruption rate and duration of emplacement calculated by considering the volume of the flow. Eruption rate is defined here as values averaged over the entire flow unit eruption time period.

However, this simple model neglects the effect of a growing crust that may impede flow advance (Kerr and Lyman, 2007; Castruccio et al., 2013). Kerr et al. (2006) showed that the cross-slope flow distance from the channel center-line (i.e., half of the channel width) can be described as a balance between parameters that contribute to flow spreading and the restraints provided by crustal cooling (Deardorff and Cashman, 2012). Depending on the lava properties and initial conditions, Kerr and Lyman (2007) showed that lava flows may stop either by an internal yield-strength or by the yield-strength of a growing surface crust. Considering that the lava flow is controlled by the yield-strength of the growing crust, we used the equations of Kerr et al. (2006) to estimate the eruption rate (Equation 10, Supplemental Material 4). This assumes that the core of the lava (below the crust) has a nearly mean pre-eruptive viscosity which is well represented by the melt's viscosity (as recalculated from its chemical composition and considering the presence of phenocrysts). The eruption rate is then converted into flow duration considering the volume of the flow.

Alternatively, we used two other approaches to estimate the flow emplacement duration and eruption rate without viscosity constraints. One is based on the relationship between eruption rate and flow length and proposes that the maximum length that a flow can reach is related to its velocity (and hence eruption rate) given the amount of heat that is lost by conduction through its thickness (Walker, 1973; Pinkerton, 1987; Pinkerton and Sparks, 1976; Pinkerton and Wilson, 1994). This is represented by the dimensionless Grätz-number, which is ~300 for most cooling-limited basaltic flows as determined by Pinkerton and Wilson (1994). Finally, we used the method of Kilburn and Lopes (1991) that is well suited for ʻaʻā and blocky lava flows to calculate their emplacement duration from their final dimensions and the reconstructed paleo-topography (Equation 12, Supplemental Material 4). Results from these three viscosity-independent methods were then converted into eruption rates and mean velocities considering the volumes of the flows.

RESULTS

Lava-Flow Characteristics, Volume, and Morphology

Deposits of the Lorenzo Plinian pumice eruption directly underlie the Nealtican lavas (Fig. 5). Neither a paleosol nor layers of reworked material indicating a significant time span lie between the lavas and the Plinian deposits, suggesting that effusive activity initiated shortly after explosive activity, maybe within a few months or years.

The lava morphology of the Nealtican lava-flow field is remarkably well preserved because of its morphological "youthfulness." Lava flows initially followed an eastward path before bending south and reaching distances up to ~17.5 km from the vent, covering an area of ~70 km^2. In the El Ombligo area, aligned spatter cones correspond to emission vents of the Nealtican lava-flow field (Figs. 1B and 2). The volume of the entire lava field was calculated at 4.2 km^3. Using area and average thickness of lavas without considering the paleo-topography, we estimated a total volume at 5.1 km^3, as a maximum-limiting volume. This is one of the largest lava fields of the Popocatépetl volcano, similar in volume to the Tochimilco lava field (5.2 km^3; Siebe et al., 2017).

In the DEMs and field observations, parts of flow units (F1–F4) have well-defined channels separated by stationary levees and delimited by discontinuous shear zones (Fig. 4). Lava surfaces within the channels exhibit thick surface ridges (ogives), which transverse to flow direction (Fig. 4), formed by a slowing flow front and buckling of a stiff surface crust (Fink, 1980).

The morphologies observed in the andesitic-dacitic flows of the Nealtican lava field correspond to block lavas with angular to subrounded blocks at centimeter to meter scale (Fig. 6A). In quarries exposing flow interior, lavas display a coherent core with basal and surface breccias (Fig. 6B). We also observed an "onion-skin" flow foliation in some cores (Fig. 6C). We also identified complex channel networks (some apparently lava-breakouts) similar to those reported for rhyolitic lava flows at Cordón Caulle volcano in Chile (Tuffen et al., 2013) and some Hawaiian ʻaʻā flows (Dietterich and Cashman, 2014). These are widely distributed along distal

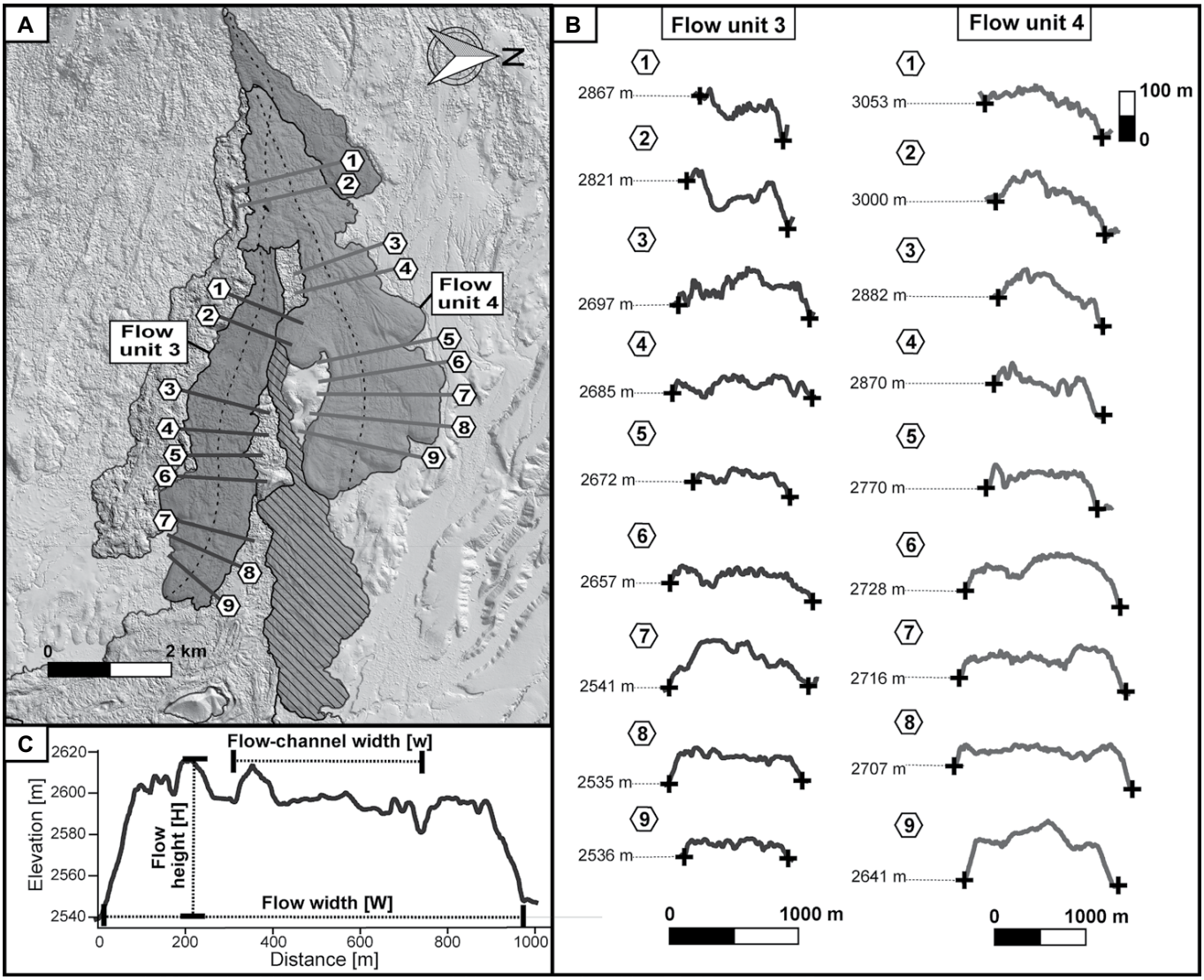

Figure 3. (A) Hillshade-DEM showing well-exposed Nealtican lava flows. Dotted line—flow centerline. The area with the line-hatch pattern was not considered in obtaining the morphological parameters. (B) Topographic profiles (perpendicular to flow direction) across well-exposed Nealtican lava flows (units F3 and F4) from which width, thickness, and channel width were estimated. Cross—lava flow margin. (C) Example of typical lava profile.

parts of F1 and F2 (Fig. 6D). Branching can be initiated at a lava-flow front or be caused by a breakout or overflow from an existing channel (Dietterich and Cashman, 2014). The lava-breakouts are typical for cooling-limited lava flows (Wilson and Head, 1994; Magnall et al., 2019). These form when internal pressure within the lava flow exceeds local confining force because of increased core pressure and/or decreased crust strength (Magnall et al., 2019). The origin of channel networks is apparently caused by interactions between advancing lava flows and topographic obstacles (Dietterich and Cashman, 2014). At Nealtican these obstacles may be hummocks (Fig. 2) of an older debris-avalanche deposit from Iztaccíhuatl volcano (Capra et al., 2002).

The occurrence of xenoliths in the lavas is also well known (e.g., Schaaf et al., 2005). They vary from a few centimeters to up to 2 m and include skarn, hornfels, anhydrite, marble, and other fragments from the local basement (Fig. 6E).

Mineralogy and Petrography

The transition from andesites to dacites occurred during the eruption, early lavas being andesites and late lavas andesites-dacites. The F3 flow is transitional, its samples are andesitic and dacitic in composition.

Lava textures of andesites (Fig. 2, units F1–F3) and dacites (units F3 and F4) are porphyritic with high modal percentages of phenocrysts (Table 1; 28.8–39.0 vol%). Micro-phenocrysts have lower percentages compared to phenocrysts (15.2–28.1 vol%). The mineral phases observed in all flows are mainly plagioclase and orthopyroxene, and in minor proportions clinopyroxene, olivine, and opaques. The groundmass contains high abundances of plagioclase and orthopyroxene microlites, and glass. Opaque minerals (<0.06 mm; 2.8–5.3 vol%) are observed in

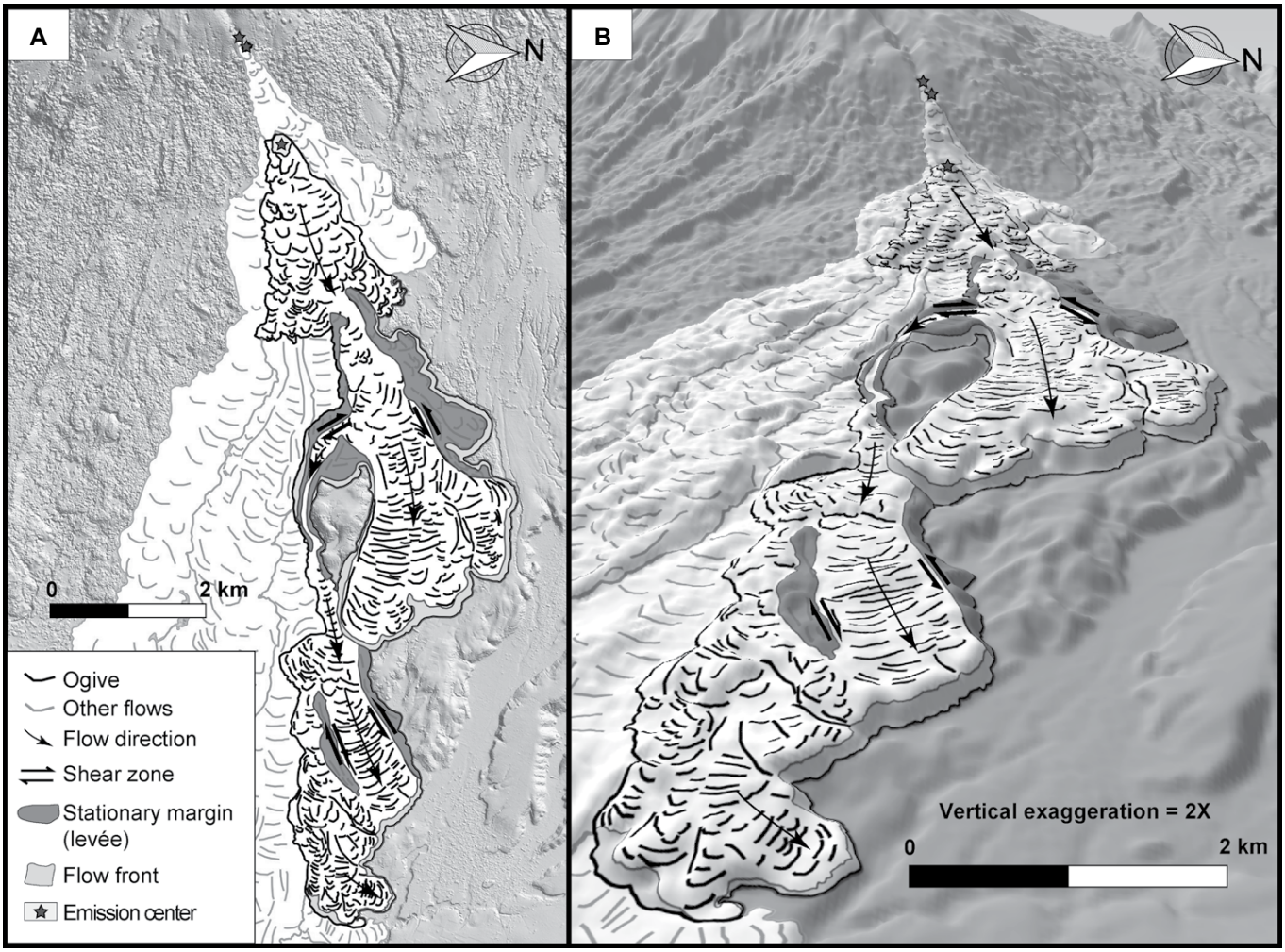

Figure 4. (A) Schematic representation of the main characteristics of the Nealtican lava flows of the Popocatépetl volcano in central Mexico. Vertical view of lava flow unit F4 (see Fig. 2). (B) Perspective view from the E of lava flow unit F4. Note the complex morphology of this flow.

all samples distributed in the groundmass and as inclusions in pyroxene and olivine crystals. Plagioclase phenocrysts (0.3–4.5 mm; in units F1–F3 = 23.9–27.3 vol% and in units F3 and F4 = 28.3–33.1 vol%) occur in a variety of types displaying (1) compositional zoning, (2) patchy cores and zoning patterns, (3) sieved zones near rims, and (4) thoroughly sieved crystals with resorption boundaries (Fig. 7A). Some pyroxene and olivine crystals also exhibit zoning. We also observed plagioclase micro-phenocrysts (in units F1–F3 = 7.6–18.6 vol% and in units F3 and F4 = 7.8–11.5 vol%) and glomero-porphyritic clusters constituted either plagioclase crystals or plagioclase with orthopyroxene, clinopyroxene, and opaques (Fig. 7B). Orthopyroxenes are observed as phenocrysts (0.3–2 mm; in units F1–F3 = 3.6–4.5 vol% and in units F3 and F4 = 4.8–6.2 vol%; Fig. 7C) and as micro-phenocrysts (in units F1–F3 = 6.7–8.2 vol% and in units F3 and F4 = 6.3–8.6 vol%), and few display minor internal dissolution features. Clinopyroxenes often have small resorption boundaries or internal sieve textures, and generally occur as phenocrysts (0.3–1.7 mm; in units F1–F3 = 0.1–1.1 vol% and in units F3 and F4 = 0.4–1.8 vol%), but sometimes as micro-phenocrysts (in units F1–F3 = 0.4–1.1 vol% and in units F3 and F4 = 0.2–0.3 vol%). Apatite occurs sparsely as inclusions in plagioclase and orthopyroxene, and olivine as isolated phenocrysts (up to 2 mm; in units F1–F3 = 0.3–1.0 vol% and in units F3 and F4 = 0.2–0.4 vol%; Fig. 7D) occasionally with skeletal shapes or within glomero-porphyritic clusters. Olivine generally contains inclusions of chromite. Some olivines have reaction rims of plagioclase, orthopyroxene, and rarely clinopyroxene and opaque minerals (Fig. 7E). In some cases, these rims display a symplectitic inter-growth of opaque minerals (Fig. 7F) which appear to be mostly magnetite. Similarly, we identified isomorphs of olivine crystals replaced by the same minerals found forming the rims. We infer that olivines are probably antecrysts inherited from a mafic magma involved in magma mixing prior to eruption (Kolisnik, 1990; Ueki et al., 2020). Trace amounts of hornblende crystals with opacite reaction rims (Fig. 7G) also occur in the dacitic flows (particularly in unit F4), together with hornblende ghosts completely recrystallized with plagioclase, pyroxene, and opaque oxides. In general, dacite samples show higher proportions of orthopyroxene phenocrysts (4.8–6.2 vol%) and lower proportions of olivine (0.2–0.4 vol%) than the andesites. The glass in the andesites has a dark and light-brown coloring, whereas in the dacites

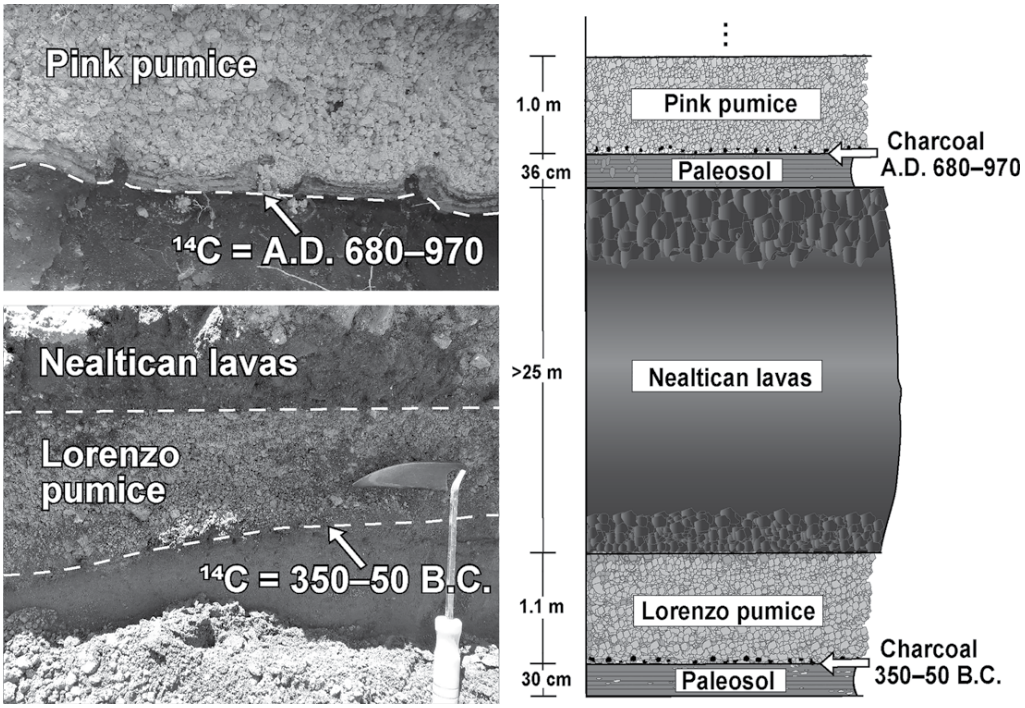

Figure 5. Schematic stratigraphic column of the Popocatépetl volcano's eruptive products cropping out on its eastern flank, relevant to this study. ^{14}C charcoal sample dates of Siebe et al. (1996a).

it is only light brown. The non-rimmed olivine crystals are present only in the andesites.

Samples also have pore spaces (0.2–14.6 vol%), some of which correspond to sub-rounded vesicles (up to 2 mm), and others to irregular inflated vesicles that originated by bubble coalescence. As in the hand specimens, in some thin sections we found skarn and hornfels xenoliths (Fig. 7H) of calc-silicate minerals associated with contact metamorphism. Most xenoliths display disequilibrium features (e.g., rounded margins), while some show thin reaction rims in contact with the host lava.

Microprobe analyses indicate that most opaque crystals in the groundmass are ilmenite, but some magnetite, and a few pyrite. Rims of olivine phenocrysts are poorer in Mg ($Fo_{77–83}$) in comparison to their cores ($Fo_{83–85}$) (Fig. 8). Crystal rim-and-core compositions of plagioclase phenocrysts and micro-phenocrysts (Fig. 8) fall mostly in the labradorite ($An_{50–64}$) and andesine fields ($An_{32–49}$). Crystal rim-and-core compositions of orthopyroxene phenocrysts and microphenocrysts fall in the enstatite field and display a wide range ($En_{55–85}Fs_{13–42}Wo_{1–4}$) in comparison to clinopyroxenes ($En_{38–46}Fs_{13–23}Wo_{38–42}$), which plot in the augite field (Fig. 8) (classification after Morimoto, 1988).

Major and Trace Element Contents

Whole-rock chemistry of 32 rock samples (Table S1, Supplemental Material 1) were plotted in a total alkali-silica (TAS) diagram (Fig. 9) (after Le Bas et al., 1986). Analytical results were normalized to 100% on an anhydrous basis before being plotted in this and subsequent diagrams. Lorenzo pumice samples (this study) and other previously published analyses (Nealtican lavas and Lorenzo pumice data from Mangler et al., 2019) are shown for comparison. Lava compositions range from andesite (units F1–F3; 61–63 wt% SiO_2) to dacite (units F3 and F4; 63–64 wt% SiO_2), with total-alkalis <6.5 wt%. They are therefore defined to be sub-alkaline by the definition of Irvine and Baragar (1971), and show a medium-K calc-alkaline trend.

This compositional change is like the evolutionary patterns displayed by other eruptions in the TMVB, e.g., andesites and dacites of Iztaccíhuatl (58–66 wt% SiO_2; Nixon, 1988b) and Nevado de Toluca (60–69 wt% SiO_2; Torres-Orozco et al., 2017) volcanoes. In comparison to the directly underlying Lorenzo Plinian pumice fallout deposit, Nealtican lavas display generally slightly higher alkali contents (Fig. 9). The geochemical data set of Mangler et al. (2019) shows the same compositional range of our Nealtican lava and Lorenzo pumice samples. Other major and trace elements (Ni, Sr, and La) were also plotted in Harker diagrams (Fig. 10) in which two groups, early (F1 and F2) and late (F3 and F4) lavas, can be discerned. Late lavas show slight negative correlations for Al_2O_3, FeO, CaO, MgO, and Sr. Early lavas generally have higher and show more dispersed concentrations in most major and trace elements, in comparison to late lavas. Lorenzo pumice patterns are more similar to the late lavas, than to the early lavas. Trace-element diagrams (Sun and McDonough, 1989; McDonough and Sun, 1995) also reveal these similarities (Fig. 11). A slightly higher fractionation of heavy rare earth elements (REE) and a slight enrichment in the mid-REE is observable in the early lavas (Fig. 11), with respect to the late lavas and Lorenzo pumices.

Both lavas and pumices display negative anomalies of Nb, Ta, and Ti, a strong positive Pb-anomaly, and a considerable enrichment in the large-ion lithophile elements (LILE) with respect to the high-field-strength elements (HFSE). These also show fractionated REE patterns, which are common in subduction environments (Hawkesworth et al., 1977; Gill, 1981). The Eu-anomaly indicative of plagioclase fractionation is almost absent (Eu/Eu* = 0.81–1.0).

Thermobarometry and Hygrometry

We calculated crystallization temperatures and pressures, as well as water-contents for all Nealtican lava-flow samples (Table S3, Supplemental Material 3). Estimated temperatures from olivine cover a range of 1119–1125 ± 45 °C at 400 MPa (pressure data from Witter et al., 2005 and Roberge et al., 2009) corresponding to depths of ∼15 km, while Fe-Ti oxides

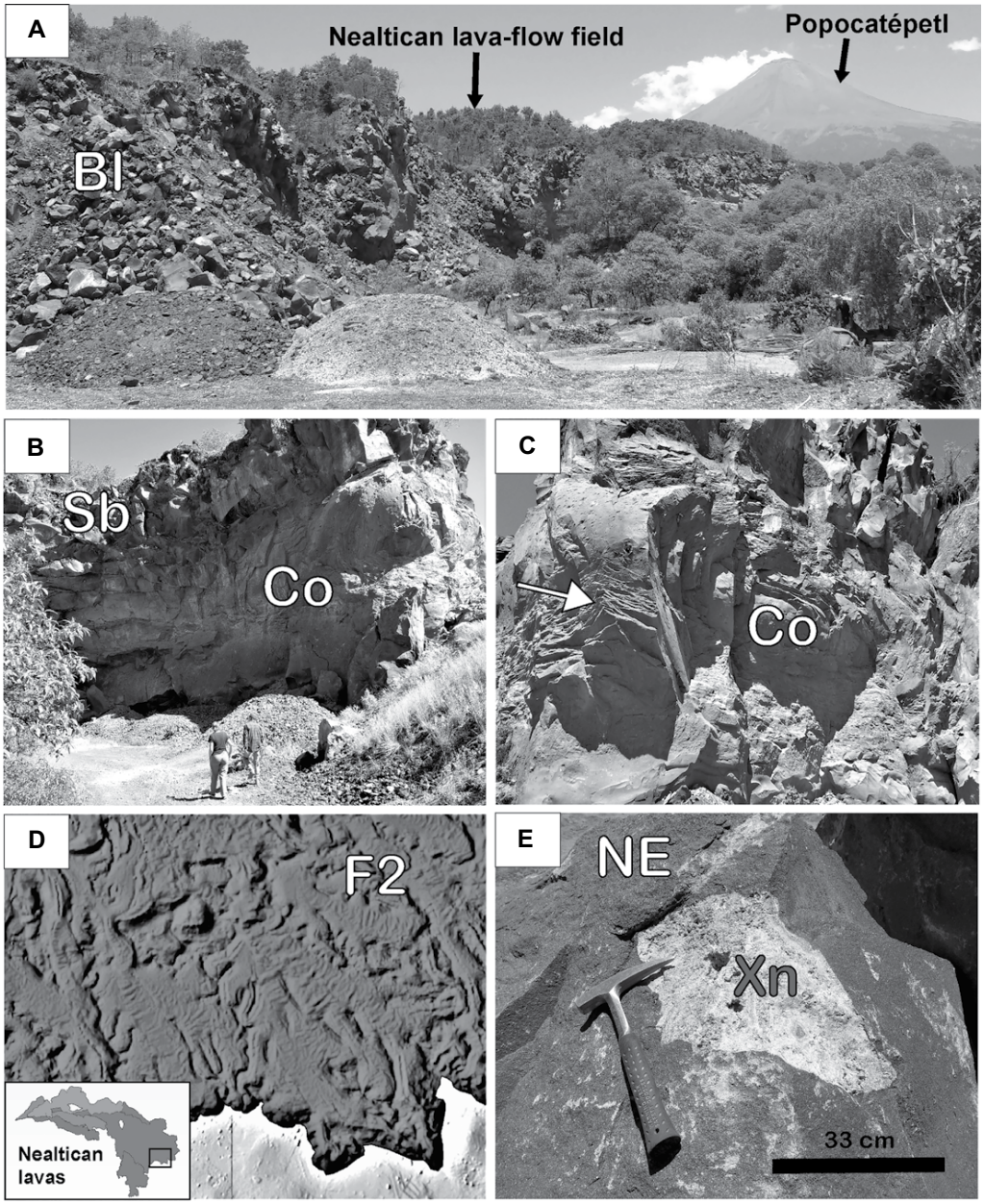

Figure 6. (A) Quarries at the eastern distal front of the Nealtican lava flow unit F2 and its characteristic surface blocks (Bl), Popocatépetl's cone appears >15 km in the distance. (B) Quarry at the lava flow front (unit F2) near the town of San Buenaventura Nealtican, Puebla, Mexico, displaying the flow's massive interior (Co) and surface breccia (Sb). (C) "Onion-skin" flow foliation (arrow) in the lava core (Co). (D) Hillshade-DEM showing complex channel networks (some appearing to be lava-breakouts widely distributed along distal parts of units F1 and F2. Inset in D indicates location of some complex channel networks. (E) Skarn xenolith (Xn) in Nealtican lava (NE) at a lava-flow front.

indicate temperatures of 925 ± 50 °C. Crystallization conditions of plagioclases in all lavas were constrained at 1040–1073 ± 36 °C at 150 MPa (pressure data from Witter et al., 2005) corresponding to depths of ~6 km, while clinopyroxenes indicate temperatures in the range of 1031–1076 ± 42 °C and pressures of 200–440 ± 150 MPa corresponding to depths of ~8–17 km. Orthopyroxenes indicate temperatures in the range of 1049–1055 ± 39 °C and pressures of 250–310 ± 260 MPa corresponding to depths of ~9–12 km. Water contents estimated using plagioclase compositions yielded a range of 0.9–1.4 ± 0.35 wt% H_2O.

Magma and Lava Rheology

We estimated the viscosity of the magma to be 3.6×10^4–4.7×10^7 Pa·s (925–1125 °C; 0.9–1.4 wt% H_2O; andesitic-dacitic compositions; Table 2), considering 29–39 vol% phenocrysts and the recalculated chemical composition (Table S5, Supplemental Material 4).

The viscosity of the lava was then obtained by also considering the micro-phenocrysts and assuming an evolved melt phase (interstitial liquid) composition, as measured in some lava samples with interstitial glass between phenocrysts (PO09, PO41, and PO18). This was done by simulating angular prolate (plagioclase) and angular equant (pyroxene and olivine) crystal shapes by applying the Costa et al. (2009) equations with the fitting parameters of Cimarelli et al. (2011; see Supplemental Material 3 for more details). At high enough strain rates (~10^{-3} s^{-1}), a maximum degree of ordering is reached and the effective viscosity is no longer strain rate-dependent (Costa et al., 2009). Considering that the samples do not have a trachytic texture, i.e., the crystals are not oriented in a preferential direction, we calculated the viscosity for a deformation rate of 10^{-4} s^{-1}. The estimated viscosity of the extruded lava yielded a

TABLE 1. MODAL MINERALOGICAL ANALYSES OF NEALTICAN LAVA-FLOW SAMPLES, POPOCATÉPETL VOLCANO, MEXICO

Sample	Flow unit	Phenocrystals*				Micro-phenocrystals*				Op (%)	Gm (%)	Vs (%)	Total (%)
		Plg (%)	Opx (%)	Cpx (%)	Ol (%)	Plg (%)	Opx (%)	Cpx (%)	Ol (%)				
PO09	F1	25.1	3.8	0.6	1.0	18.6	8.2	1.1	0.2	4.3	28.5	8.6	100
PO41	F1	26.1	3.6	1.1	0.3	14.3	7.1	0.4	—	3.6	33.7	9.8	100
PO44	F2	27.3	4.5	0.1	—	9.8	7.3	0.8	—	4.5	41.9	3.8	100
PO54	F2	24.3	4.0	0.6	0.8	10.8	6.7	0.5	0.1	2.8	34.8	14.6	100
PO32	F3	23.9	3.6	0.8	0.5	7.6	7.1	0.5	—	5.3	39.2	11.5	100
PO28	F3	33.1	4.8	0.8	0.3	11.5	6.4	0.2	—	3.7	39.0	0.2	100
PO16	F4	29.0	6.2	0.6	0.2	9.2	6.3	0.3	—	3.2	39.7	5.3	100
PO24	F4	28.3	5.0	1.8	0.4	7.8	7.0	0.2	—	2.8	35.7	11.0	100
PO18	F4	31.1	5.3	0.4	—	9.3	8.6	—	—	3.9	37.6	3.8	100

*Abbreviations: Plg—plagioclase; Opx—orthopyroxene; Cpx—clinopyroxene; Op—opaque minerals; Gm—groundmass; Vs—vesicles. Phenocrysts (≥0.3 mm), micro-phenocrysts (<0.3–0.15 mm). Amphibole is too scarce to be taken into account.

range of 1.1×10^9–4.1×10^{10} Pa·s (1055–1071 °C; 0.1 wt% H_2O; 45–59 vol% phenocrysts and micro-phenocrysts; Table 2) for the andesitic lavas (units F1–F3) and of 1.1×10^{11}–1.4×10^{12} Pa·s (925–1049 °C; 0.1 wt% H_2O; 52–58 vol% phenocrysts and micro-phenocrysts; Table 2) for dacitic lavas (units F3 and F4).

Eruption Rate and Emplacement Duration

All morphological parameters for units F3 and F4 are given in Table 3 and below we present a summary of the eruption rates, velocities, and emplacement times of the Nealtican lava flows as calculated by the morphology-based methods (Table 4). We used the lava viscosities from the petrological analyses of the lava flow samples ($\eta_{meanF3} = 5.5 \times 10^{10}$ and $\eta_{meanF4} = 1.0 \times 10^{12}$ Pa·s; Table 2) and the Jeffreys (1925) equation (Equation 5, Supplemental Material 4), the measured flow thicknesses, slope angles of ~4° and ~5°, and densities of 2565 kg/m^3 (andesites) and 2402 kg/m^3 (dacites), respectively, and we infer flow velocities to have been 4 and 1 m/day for units F3 and F4, respectively (Table 4). We consider the volumes of the flows obtained from their average width and their length (F3 = ~6.5×10^8 m^3 and F4 = ~1.0×10^9 m^3), these volumes convert to eruption rates of 3 and 1 m^3/s and emplacement durations of 6 and 29 years for units F3 and F4, respectively (Table 4).

If the flow dynamics are controlled by the effect of a lava's growing crust, we can estimate the eruption rate by assuming a yield strength of the crust of 2×10^6 Pa (best fit from Kerr and Lyman, 2007) and viscosity of the lava flow core (pre-eruptive conditions: $\eta_{meanF3} = 2.9 \times 10^6$ and $\eta_{meanF4} = 3.1 \times 10^7$ Pa·s; Table 2). Results give eruption rates of 15 and 8 m^3/s, which convert into flow velocities of 20 and 5 m/day, and emplacement durations of 1 and 4 years for units F3 and F4 (Table 4), respectively.

Alternatively, the eruption rates obtained through the Grätz-number approach are much higher and yields values of 19 and 13 m^3/s for units F3 and F4, respectively. These convert into emplacement durations of 1 and 2 years which corresponds to average lava advances of 25 and 7 m/day (Table 4).

Finally, by the model of Kilburn and Lopes (1991), emplacement durations range from 1 to 5 years for units F3 and F4 (Table 4), respectively. By the lava flow volumes, these values convert into eruption rates of 25 and 6 m^3/s and advancement velocities of 33 and 4 m/day, respectively. Error-propagation calculations (following Lefler, 2011 and Chevrel et al., 2013) for eruption rates, velocities, and emplacement times of these models yield an error of up to 17%.

DISCUSSION

Magma Source and Evolution

Samples from the Nealtican lavas provide evidence that allowed us to distinguish two different magma batches that produced the early (units F1 and F2) and late lava (units F3 and F4) groups. These groups are distinguishable by their SiO_2 content, concentrations of major and trace elements, mineral proportions, and textural characteristics. This is also evident in the Nealtican isotopic compositions (Fig. 12) from Mangler et al. (2019). On Harker diagrams (Fig. 10), many major element oxide concentrations decrease toward silicic compositions, so we infer that dacite represents a felsic end-member. The high FeO, MgO, and Ni concentrations in the early lavas suggest the presence of a mafic end-member. Consequently, the andesites would be a hybrid product that resulted from the mixture of a dacitic and a basaltic/basaltic-andesitic component in a magma chamber (Schaaf et al., 2005; Roberge et al., 2009; Mangler et al., 2019). This is supported by our microprobe data (Table S2, Supplemental Material 2, Fig. 7), which shows a large range of mineral compositions. The most convincing evidence for the occurrence of magma-mixing prior to eruption stems from the textures and mineralogy of the volcanic products. Many crystals show textures of corrosion-reaction and zoning that demonstrate a complex transit, far from equilibrium, within the magmatic system. In fact, in the Nealtican samples we found olivine phenocrysts with reaction rims and abundant disequilibrium textures resulting from the mixing between mafic and silicic magmas (Larocque et al., 1998; Coombs and Gardner, 2004), as observed before in Popocatépetl products (e.g., Sosa-Ceballos et al., 2014). This is also supported by plagioclase textures (sieve textures, resorption rims, and zoning). The olivine range of the Nealtican samples indicates different magma residence times and the presence of multiple injections of mafic magma into a reservoir (Ueki et al., 2020).

The increase in highly incompatible element abundances such as the light-REE and Th with increasing SiO_2 (e.g., La vs SiO_2 shown in Fig. 10) in the late lavas is consistent with fractional crystallization. In contrast, the early lavas (Fig. 10) show more dispersed concentrations in major and trace element plots, that resulted from magma mixing.

A typical feature of Popocatépetl rocks is that they commonly exhibit evidence of magmatic interaction with the basement and upper-crustal rocks (xenoliths of skarn, meta-siltstone, marble, anhydrite, granodiorite, diorite, gabbro, etc.), which could also slightly modify the isotopic composition of the volcanic products (Goff et al., 2001; Schaaf et al., 2005; Gómez-Tuena et al., 2005; Sosa-Ceballos et al., 2012). The isotopic data of Nealtican lavas and Lorenzo pumice from Mangler et al. (2019) indicate a negative correlation of $^{87}Sr/^{86}Sr$ versus $^{143}Nd/^{144}Nd$ ratios (Fig. 12). We compare this data with granodiorite values (Schaaf et al., 2005; Mangler et al., 2019) and the most primitive sample of the Popocatépetl edifice reported to date (Mangler et al., 2019). Andesitic compositions are closer to the isotope ratios of these samples and the Lorenzo pumice is directly genetically related to the Nealtican lavas. We also use the Th/Nb and Nb/U vs SiO_2 diagrams (Larrea et al., 2019; Fig. 12) and notice an increase in Th/Nb and a decrease in Nb/U ratios with increasing SiO_2, with values close to those of the bulk continental crust (Rudnick and Gao, 2003). These correlations are more evident in the andesites. Schaaf et al. (2005) also indicate that this overlap may correspond to comagmatic plutonic rocks from the margin of the magma chamber or earlier emplaced plutons. Sosa-Ceballos et al. (2014) and Mangler et al. (2019) indicate that skarn assimilation is not consistent with the compositional range in the Popocatépetl volcano samples by the assimilation and fractional crystallization (AFC) model of DePaolo (1981). CaO concentrations are not high in the samples, as would be

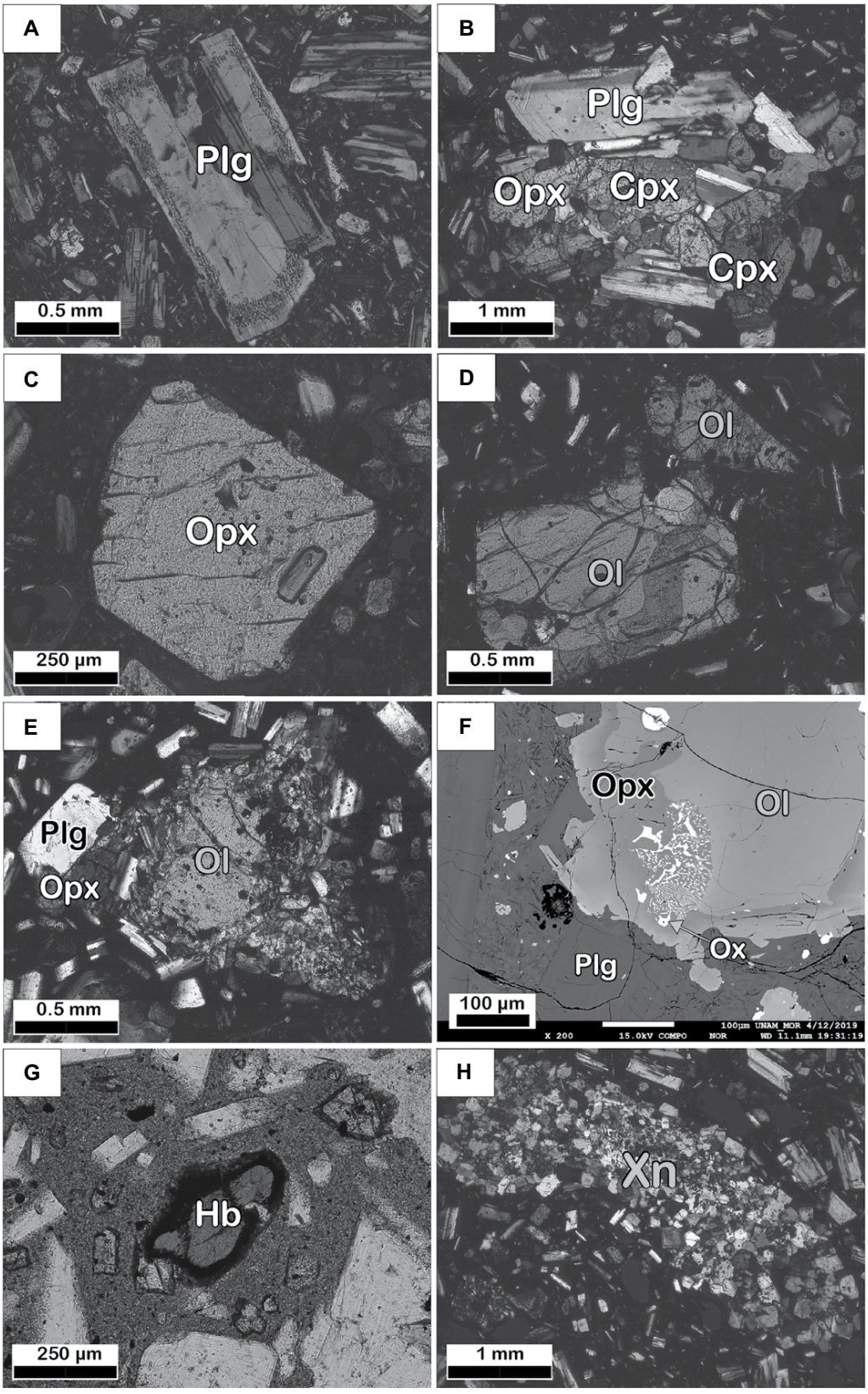

Figure 7. Photomicrographs under petrographic microscopy and an electron microprobe of Nealtican lava rock samples. (A) Idiomorphic plagioclase with sieve-texture rim (sample PO06B). (B) Glomero-porphyritic aggregate of plagioclase (Plg), orthopyroxene (Opx), and clinopyroxene (Cpx) phenocrysts (sample PO09). (C) Orthopyroxene crystal with apatite inclusion (sample PO13). (D) Idiomorphic olivine with characteristic fractures (sample PO06B). (E) Olivine (Ol) crystal with plagioclase (Plg) and orthopyroxene (Opx) reaction rim (sample PO18). (F) Back-scattered electron microscope (BSE) image of an olivine crystal with pyroxene reaction rim and development of symplectitic intergrowth of oxides (Ox) (sample PO18). (G) Hornblende with opacite reaction rim (Hb; sample PO24). (H) Hornfels xenolith (Xn) with high content of plagioclase, corundum, and opaque minerals (sample PO41). Except for F and G, all photos are under cross-polarized light.

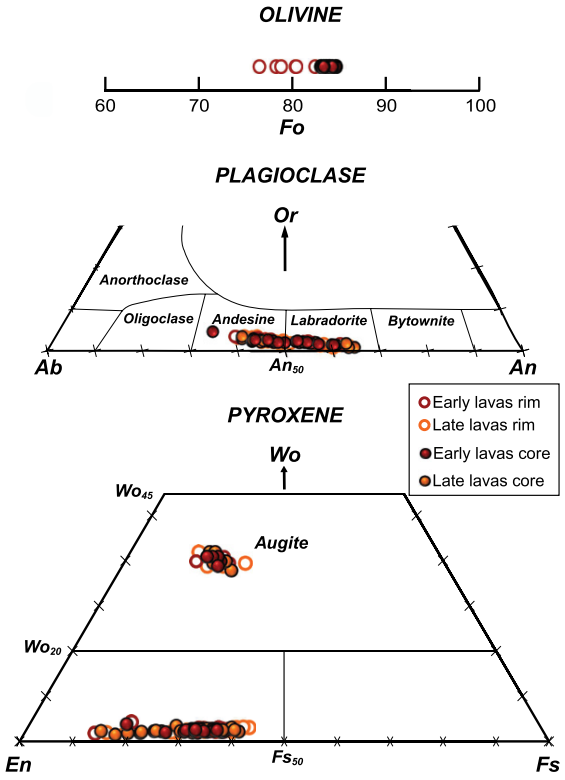

Figure 8. Mineral compositions (olivine, plagioclase, and pyroxene) in representative rock samples of the Nealtican lava flow. Pyroxene classification after Morimoto (1988).

expected in magmas interacting with carbonates on a large scale as at Vesuvius (central Italy) volcano (Jolis et al., 2015). Limestones seem to be a convincing source of the large CO_2 emissions (Goff et al., 2001; Witter et al., 2005), but it has also been proposed that mafic magma recharge could be responsible for them (Roberge et al., 2009). The origin of these high emissions might stem from both processes.

Consequently, magma-mixing and fractional crystallization are the main processes controlling the differentiation of the Nealtican lavas. Crustal assimilation could have also occurred in the reservoir, but there is no substantial data to indicate that this occurred on a large scale.

Eruption Dynamics and Eruptive Model

The Lorenzo eruption began with a sustained Plinian column (Fig. 13A) that reached heights of 20–30 km (Panfil et al., 1999) producing abundant pumice fallout (Lorenzo pumice) distributed east of the crater where it heavily affected at least ~240 km^2 (Siebe et al., 1996a). Months or years later, this explosive activity was followed by an effusive phase (Fig. 13B), the Nealtican lava flows. The change of eruption dynamics from Plinian to effusive was likely due to efficient degassing of the magma during the Plinian phase. A nearly closed system became an open system through which degassed magma could further rise through the upper crust to the surface.

Nguyen et al. (2014) indicate that degassing by itself is not always sufficient to promote the transition to effusive activity, which could also be a consequence of larger changes in the magma ascent rate. Magma ascent and decompression rates (both usually coupled) appear to be the most critical parameters controlling eruption style (Gonnermann and Manga, 2007; Cassidy et al., 2018). Thus, the change from explosive to effusive activity is caused by a decrease in the magma ascent and decompression rates. The magma supply rate of the Lorenzo Plinian eruption was probably >10^7 kg/s, as typical for Plinian eruptions (Cashman, 2004), while the estimated value for the Nealtican lavas is 10^3–10^4 kg/s. The latter is consistent with direct observations of active viscous flows and domes (Pioli et al., 2009). Scarce amphibole phenocrysts in equilibrium can be found in silicic pumice clasts and Rutherford (2008) suggests that these crystals indicate rapid magma mixing and ascent. In contrast, amphibole crystals in dacitic lavas usually display thick decompression reaction rims, in this case Rutherford and Hill (1993) indicate that their ascent and decompression rate was much slower. Yet some crystals are completely replaced by plagioclase, pyroxene, and opaques, very similar to those reported by De Angelis et al. (2015) and Peters et al. (2017). So, these may be antecrysts in textural disequilibrium with the host magma (heating related to mixing processes).

Based on our thermobarometric (Table S3, Supplemental Material 3) and petrological information, we propose a model (Fig. 13) in which a mafic magma rises from the mantle through the thick crust and arrives first at a deeper reservoir (8–17 km). This magma (with olivine, pyroxene, and amphibole) subsequently reaches a shallower (~6 km) more differentiated felsic reservoir (with plagioclase, ± pyroxene, and Fe-Ti oxides) that has undergone fractional crystallization and minor assimilation. This second reservoir is hosted in Cretaceous limestones, where it generates a skarn-type contact aureole (Fig. 6E). Injection of the more mafic magma into the felsic magma triggers convection and mixing, and produces the observed crystal disequilibrium textures and a hybrid andesitic magma composition. Oversaturation of volatiles (e.g., CO_2) and vesiculation caused by magma-mixing increases magma pressure (Sparks et al., 1977), which may be sufficient to fracture the reservoir boundaries, incorporate xenoliths from the upper

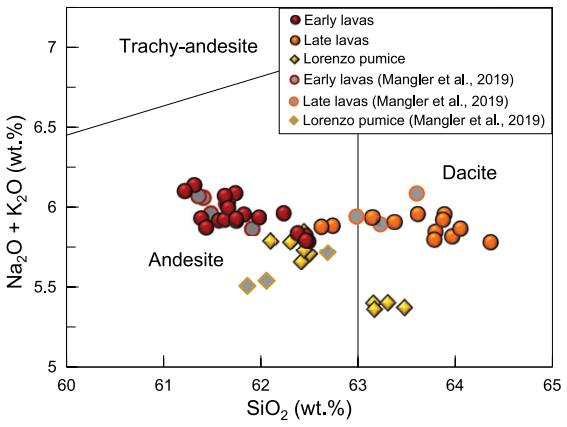

Figure 9. Nealtican lava rock-sample compositions (red and orange circles) plotted in a total alkali versus silica (TAS) diagram (analyses recalculated to 100% on a H_2O-free basis) after Le Bas et al. (1986). Early and late flows can be distinguished. Lorenzo pumice samples (yellow diamonds) and other previously published analyses (gray circles for Nealtican lavas and diamonds for Lorenzo pumice; data from Mangler et al., 2019) are shown for comparison.

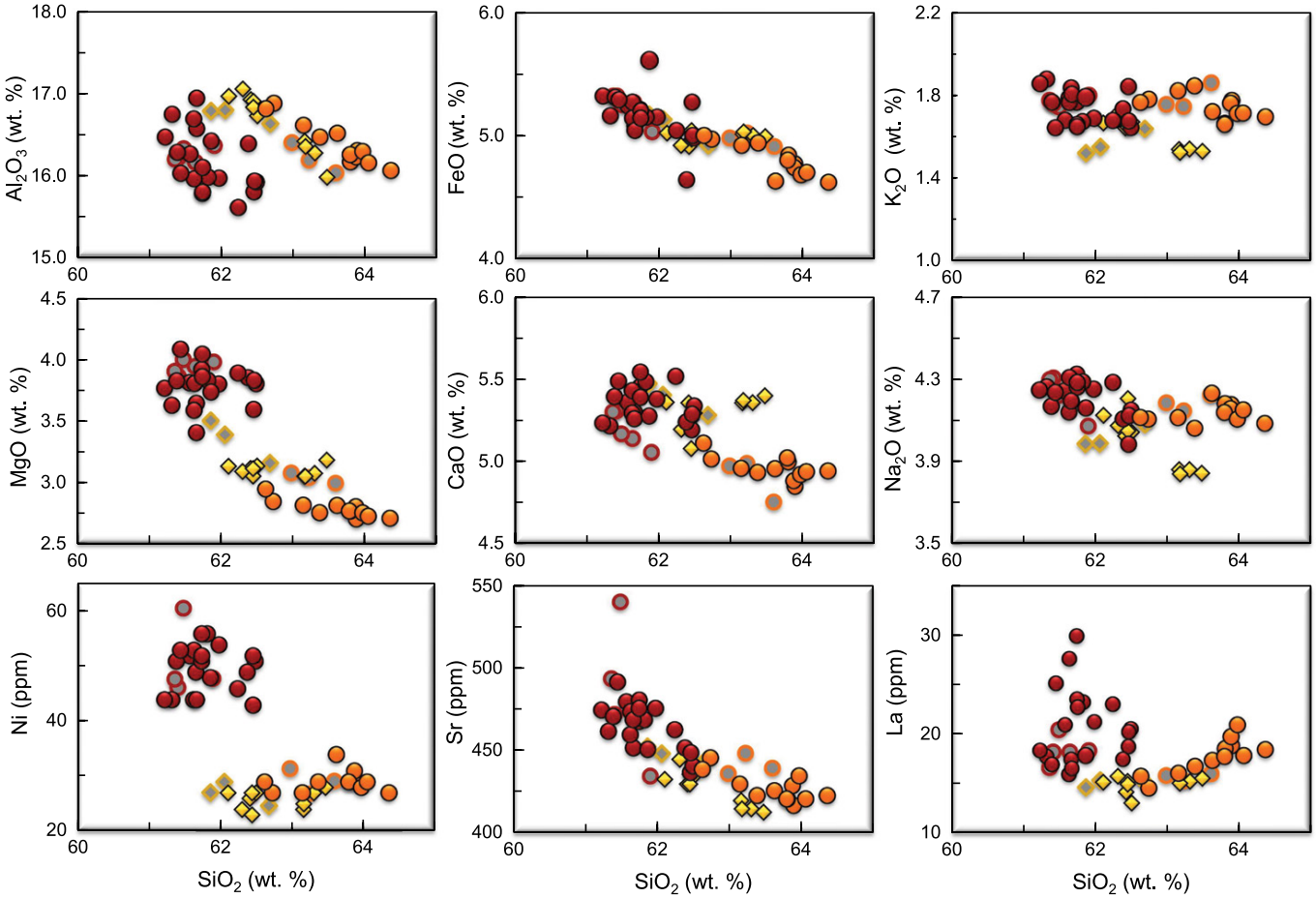

Figure 10. Harker diagrams of Nealtican lava rock-samples showing selected major (wt%) and trace (ppm) elements plotted against silica (symbols and data sources as in Fig. 9).

crust (skarn, marble, etc.), and trigger an explosive eruption in the summit vent (Fig. 13A; Plinian activity). It is highly probable that at the end of this activity a dome was formed in the summit vent. Finally, a decrease in the magma ascent and decompression rates coupled with an efficient gas-loss leads to a change in the eruption style (from explosive to effusive) producing the Nealtican lava-flow field (Fig. 13B). A dome blocking the summit vent may have forced the magma to seek for an alternative path to the surface. As a result, Nealtican lavas were extruded along the NE-SW Atexca fault through the aligned El Ombligo flank vents suggesting that the magma was transported from a shallow reservoir to the surface through a dike system (Fig. 13B). Such a system probably had a low overpressure during magma ascent, which according to Geshi et al. (2020) also promotes an effusive eruption (e.g., Miyakejima volcano, Japan). The less viscous andesitic magma propagated first through dikes and erupted before the more viscous phenocryst-rich dacitic magma, because low-viscosity magmas have a higher eruptibility than viscous ones (Takeuchi, 2011).

Lava-Flow Viscosity

The rare occurrence of active lava flows of evolved composition causes a gap in our knowledge partly filled by estimates based on the lavas' morphology and petrology (e.g., Castruccio et al., 2013; Dietterich et al., 2018; Takeuchi, 2011), and by experimental determinations (e.g., Castruccio et al., 2010; Del Gaudio et al., 2013).

Our study ignores effects of bubbles to avoid complexities related to three-phase mixture models that have not been sufficiently explored to describe a general law (Pistone et al., 2016). Yet the experimental study of Pistone et al. (2012), with a wide range of crystallinities (24–65 vol%) and limited bubble contents (9–12 vol%), shows that addition of relatively small bubble volume fractions to particle-bearing suspensions significantly decreases magma viscosities (Pistone et al., 2016). Our viscosity estimates may thus be overestimated. They are first-order approximations that do not take into account heterogeneities in the distribution of crystals and bubbles, crystal interactions, etc. (Caricchi et al., 2007; Costa et al., 2009; Lavallée et al., 2007; Chevrel et al., 2016b). We obtain magma (pre-eruptive conditions) viscosities of 10^4–10^5 Pa·s for andesites, while for dacites we obtain values in the range of 10^6–10^7 Pa·s. These data are within the range of estimations of pre-eruptive viscosities for andesitic (10^4–10^5 Pa·s at Pinatubo (Philippines) and Colima (Mexico) volcanoes; Takeuchi, 2011) and dacitic magmas (10^7 Pa·s at Pinatubo and Mount Rainier (Washington, USA) volcanoes; Takeuchi, 2011). Viscosity values for the andesitic Nealtican lavas at eruptive conditions (10^9–10^{10} Pa·s) cover the same range of magnitudes as those reported for other andesitic subduction-related volcanoes such as Colima stratovolcano (10^9–10^{10} Pa·s; Navarro-Ochoa et al., 2002), and Rancho Seco (Michoacán, Mexico) monogenetic scoria cone (10^8–10^9 Pa·s; Ramírez-Uribe et al., 2021). Our

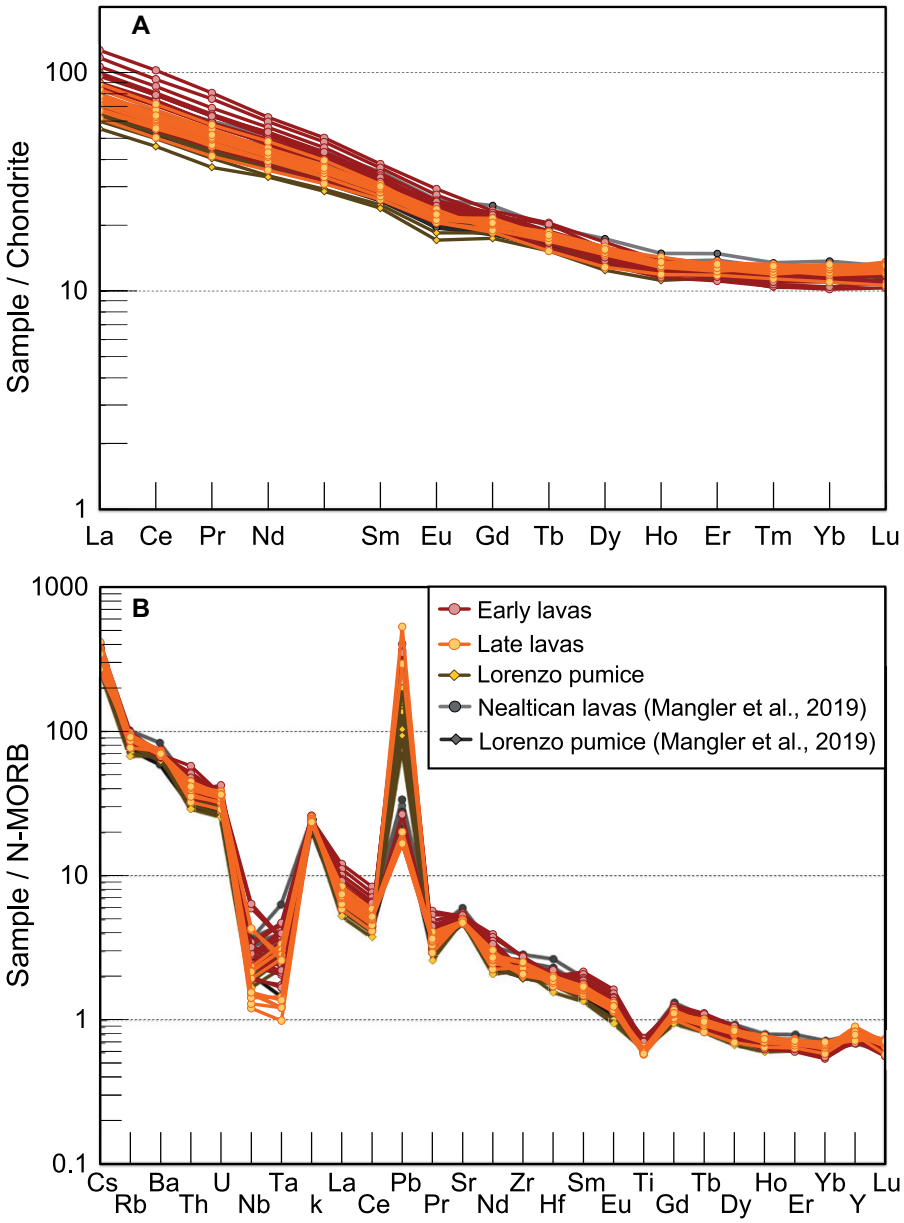

Figure 11. (A) Chondrite-normalized rare earth element (REE) plot (after McDonough and Sun, 1995) for Nealtican rock samples. (B) N-MORB trace element patterns (after Sun and McDonough, 1989) for Nealtican rock samples. Early and late flows can be distinguished. Lorenzo pumice samples (in yellow-ochre) and other previously published analyses (in gray for Nealtican lavas and Lorenzo pumice; data from Mangler et al., 2019) are shown for comparison. N-MORB—Normal mid-ocean ridge basalt.

viscosity estimated for dacitic flows (10^{11}–10^{12} Pa·s) is similar to other dacitic volcanoes such as Santiaguito volcano (10^{10} Pa·s; Harris et al., 2002). Syn-eruptive viscosities (10^{9}–10^{12} Pa·s) are five orders of magnitude more viscous in comparison to pre-eruptive values of andesitic-dacitic compositions (10^{4}–10^{7} Pa·s), which is mainly the result of volatile loss, cooling, and increased crystallinity. Nevertheless, magma mixing also plays a role in producing less viscous magmas that may trigger an eruption (Takeuchi, 2011). At depth, mushy plutons can be mobilized by the addition of volatiles (mainly H_2O) and heat released by ascending hydrous mafic magmas that induce a significant decrease of their bulk viscosity and potentially their density (Bachmann and Bergantz, 2008; Pistone et al., 2012).

Flow-Emplacement Conditions and Duration of Eruption

Active andesitic-dacitic flows of the dimensions of the Nealtican lava field have not been observed by volcanologists, which makes it difficult to define their emplacement mode. Nevertheless, from lava flow morphological characteristics, the eruption rates and the emplacement times are approximated for flows F3 and F4 (Table 4), and employed to roughly calculate the total time that was required to emplace the Nealtican lava volume (4.2 km^3). Approximately 3.2 km^3 of this volume corresponds to andesite (units F1–F3) and 1.0 km^3 to dacite (unit F4). Note that unit F3 is transitional in composition. We do not consider pauses that might have occurred, and assume that each flow was erupted one after the other, not simultaneously. If so, the successive emplacement of the andesitic flows probably took from 4 (by a mean maximum eruption rate of 25 m^3/s from the Kilburn and Lopes model) to 31 years (by a mean minimum eruption rate of 3 m^3/s from the Jeffreys equation). Meanwhile, the emplacement of the dacitic flows required from 3 (by a mean maximum eruption rate of 13 m^3/s from the Grätz-number model) to 29 years (by a mean minimum eruption rate of 1 m^3/s from the Jeffreys equation). Accordingly, the total emplacement of the Nealtican lavas could have taken 8–59 years. Eruption rates obtained for the Nealtican andesite lava flows (3–25 m^3/s) are similar to those reported from other subduction-related volcanoes with comparable compositions such as Paricutin (1.5–14 m^3/s; Larrea et al., 2017), Malpaís de Zacapu (2–14 m^3/s; Reyes-Guzmán et al., 2021), Rancho Seco (2–19 m^3/s; Ramírez-Uribe et al., 2021), Sinabung (Sumatra, Indonesia) (1–20 m^3/s; Pallister et al., 2019), and Soufrière Hills (Montserrat, UK) (>5 m^3/s; Watts et al., 2002). Likewise, eruption rates for the Nealtican dacitic lava flows (1–8 m^3/s; excepting the high value of 13 m^3/s obtained by the Grätz-number model) are similar to those previously reported for Santiaguito volcano (0.5–1.6 m^3/s; Harris et al., 2002, 2004), the Chao lava flow (Chile) (5–8 m^3/s; De Silva et al., 1994), and the Unzen dome (Japan) (4.6 m^3/s; Nakada and Motomura, 1999).

Neither the Grätz-number nor the Kilburn and Lopes models take into account internal lava rheology, which can play an essential role in the behavior of lava flows (Castruccio et al., 2013). Given that these highly crystalline lava flows likely did not behave as a Newtonian fluid but as a yield strength-controlled flow (Castruccio

TABLE 2. MAGMA AND LAVA VISCOSITIES ESTIMATED BY PETROLOGICAL APPROACH, NEALTICAN LAVA-FLOW SAMPLES, POPOCATÉPETL VOLCANO, MEXICO

Sample	Flow unit	Composition	Pre-eruptive conditions					Syn-eruptive conditions (0.1 wt% H_2O)			
			T (°C)	wt% H_2O	Melt viscosity (Pa·s)	Relative viscosity	Apparent viscosity (Pa·s)	T (°C)	Melt viscosity (Pa·s)	Relative viscosity	Apparent viscosity (Pa·s)
PO09	F1	Andesite	1125	0.9	2.4E + 03	2.3E + 01	5.5E + 04	1065	1.2E + 06	3.6E + 04	4.1E + 10
PO41	F1	Andesite	1119	1.0	1.7E + 03	3.4E + 01	5.8E + 04	1064	1.9E + 06	1.1E + 04	2.1E + 10
PO54	F2	Andesite	1124	0.9	2.2E + 03	1.6E + 01	3.6E + 04	1071	1.6E + 06	1.9E + 03	3.0E + 09
PO32	F3	Andesite	1055	1.3	6.6E + 03	1.6E + 01	1.1E + 05	1055	2.3E + 06	4.6E + 02	1.1E + 09
PO28	F3	Dacite	1049	1.3	9.3E + 03	6.1E + 02	5.7E + 06	1049	2.7E + 06	4.0E + 04	1.1E + 11
PO18	F4	Dacite	925	1.3	1.7E + 05	2.8E + 02	4.7E + 07	925	1.1E + 08	1.3E + 04	1.4E + 12
PO16	F4	Dacite	925	1.4	1.2E + 05	1.3E + 02	1.5E + 07	925	1.1E + 08	5.8E + 03	6.4E + 11

TABLE 3. MORPHOLOGIC FLOW PARAMETERS OF NEALTICAN LAVA-FLOW UNITS, POPOCATÉPETL VOLCANO, MEXICO

Parameter	Unit F3	stdev	Unit F4	stdev
Flow width W [m]	985	0.30	1505	0.50
Channel width w [m]*	577	0.41	788	0.003
Length L [m]	10,031	0.87	6,739	0.08
Thickness H [m]	66	2.07	101	5.79
Slope Θ [°]	4.4	0.005	5.3	0.004
Volume (LWH) [m³]†	6.54E + 08	2.04E + 07	1.02E + 09	5.87E + 07

Notes: stdev—standard deviation.
*Obtained only with 4 and 2 profiles for units F3 and F4, respectively.
†Volume = L × W × H.

et al., 2013) or even as a glacier-like flow (that means the flows are plug-dominated and might be slipping on a basal layer; Latutrie et al., 2017), the Jeffreys method seems the least appropriated in this case, but it provides an upper limit. We believe that consideration of the yield strength in a growing-crust regime and resulting time value might be more realistic for the emplacement mode of the Nealtican andesitic lavas, since the occurrence of flow breakouts indicates the presence of a surface crust (Tuffen et al., 2013; Farquharson et al., 2015; Magnall et al., 2017). At the same time, the eruption rates estimated for dacites by the Jeffreys equation are more consistent with those from observed active dacitic lavas (Harris et al., 2002, 2004). Castruccio et al. (2013) indicate that it is more convenient to consider the yield strength of the flow's core for these types of lava flows. Taking into account all the above considerations, we propose a more realistic time of ∼35 years for emplacement of the entire Nealtican lava field. Comparing with directly observed eruptions that produced andesitic lava fields, the Paricutin eruption (1943–1952) lasted much less (∼9 years; with a volume of only 1.7 km³; Larrea et al., 2017), but the andesitic part of Nealtican represents almost twice this volume. Likewise, the Lonquimay 1988–1990 andesitic flow (∼0.23 km³) with a total emplacement duration of 330 days (Naranjo et al., 1992), represents only 7% of the andesitic volume of the Nealtican lava-flow field. In fact, flow-front velocities of the Nealtican lavas fall in the range reported for the Lonquimay 1988–1990 lavas. Eruption rates decreased over time in some witnessed andesitic eruptions (e.g., Naranjo et al., 1992; Larrea et al., 2017; Carr et al., 2019), a pattern not considered in our work. Furthermore, some flows have been observed to continue advancing after eruption cessation (e.g., the 2011–2012 Cordón Caulle lava flow, Chile; Tuffen et al., 2013; Magnall et al., 2017).

The estimated mean lava flow velocities of 1–33 m/day indicate that lava fronts did advance relatively slowly and would not represent a danger for onlooking populations. Yet depending on the location of a future vent, a similar eruption could cause great damage to the infrastructure of present towns (e.g., Santiago Xalitzintla, San Nicolás de los Ranchos, San Baltazar

TABLE 4. SUMMARY OF ERUPTION RATES, VELOCITIES, VISCOSITIES, AND EMPLACEMENT TIMES OF NEALTICAN LAVA-FLOW UNITS, POPOCATÉPETL VOLCANO, MEXICO, CALCULATED BY MORPHOLOGY-BASED METHODS

Viscosity (Pa·s)	Eruption rate (m^3/s)	% error*	Mass eruption rate^{QM} (kg/s)	Velocity (m/day)	% error	Time (years)	% error	Method
Unit F3								
5.5E+10$^{\eta a}$	3^{Qu}	12	8.5E + 03	4^{uJ}	11	6^{tV}	12	Jeffreys equation
2.9E+06$^{\eta L}$	15^{Qw}	7	3.8E + 04	20^{uQ}	7	1^{tV}	7	Kerr et al. (2006)
—	19^{QGz}	3	4.8E + 04	25^{uQ}	4	1^{tV}	4	Grätz-number
—	25^{QV}	3	6.5E + 04	33^{uQ}	4	1^{tKL}	9	Kilburn and Lopes (1991)
Unit F4								
1.0E+12$^{\eta a}$	1^{Qu}	16	2.7E + 03	1^{uJ}	15	29^{tV}	17	Jeffreys equation
3.1E+07$^{\eta L}$	8^{Qw}	5	2.0E + 04	5^{uQ}	7	4^{tV}	7	Kerr et al. (2006)
—	13^{QGz}	6	3.1E + 04	7^{uQ}	8	3^{tV}	8	Grätz-number
—	6^{QV}	6	1.5E + 04	4^{uQ}	8	5^{tKL}	12	Kilburn and Lopes (1991)

$^{\eta a}$Apparent viscosity of petrological approach. Viscosity in syn-eruptive conditions.
$^{\eta L}$Liquid viscosity with Giordano et al. (2008). Viscosity in pre-eruptive conditions.
^{Qu}Estimated with Q = uWH. Equation (7) of Supplemental Material 4.
^{Qw}Estimated with Eq. (10) of Supplemental Material 4 using liquid viscosity. Yield strength in a growing crust regime of Kerr et al. (2006) with $\sigma_c = 2E + 06$ Pa (best fit of Kerr and Lyman, 2007).
^{QGz}Estimated with the Grätz number method. Equation (8) of Supplemental Material 4.
^{QV}Estimated with Eruption rate = Volume/Time.
^{QM}Estimated with Mass eruption rate = Eruption rate × density.
^{uJ}Estimated with Jeffreys Equation (5) of Supplemental Material 4 using apparent viscosity of petrological approach.
^{uQ}Estimated with u = Q/WH, re-organized Equation (7) of Supplemental Material 4.
^{tV}Estimated with Time = Volume/Eruption rate.
^{tKL}Estimated with Equation (12) of Supplemental Material 4. Emplacement time of Kilburn and Lopes (1991).
*Error-propagation calculated following Lefler (2011) and Chevrel et al. (2013).

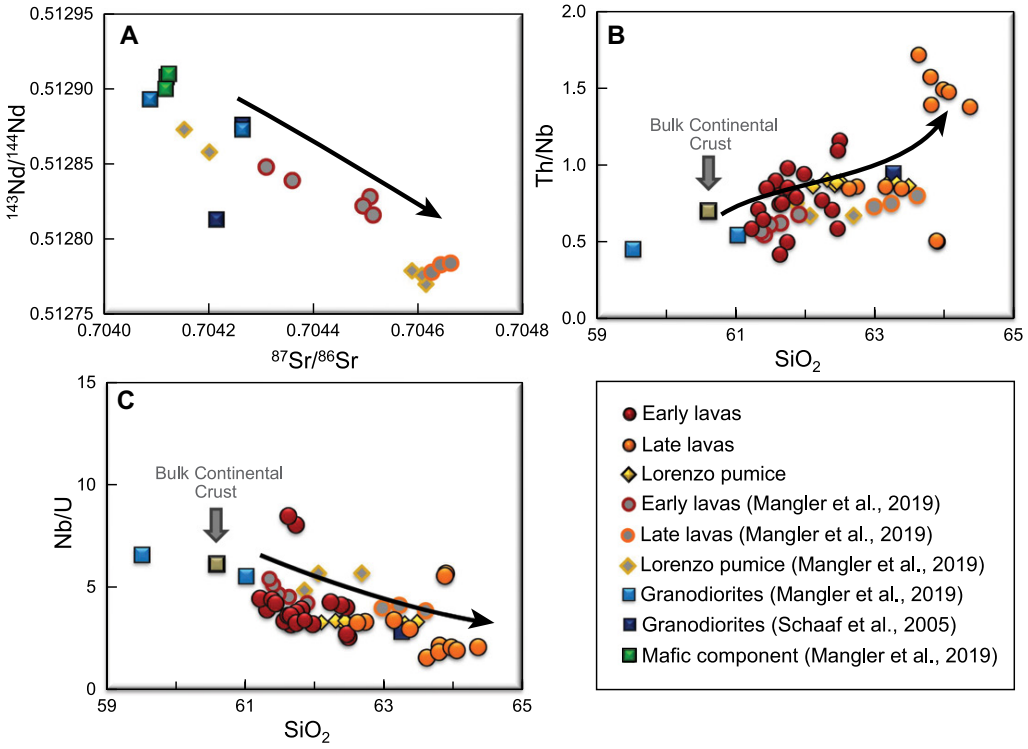

Figure 12. (A) Nd-isotope ratios versus SiO_2 (wt%). Samples of the most mafic component of Popocatépetl volcano are included (green squares; data from Mangler et al., 2019). (B) Th/Nb ratios versus SiO_2 (wt%) for the Nealtican lavas analyzed in this study, Lorenzo pumice data (this study) and from the literature (Mangler et al., 2019). For comparison we show the bulk continental crust trace element ratios (from Rudnick and Gao, 2003). (C) Nb/U ratios versus SiO_2 (wt%) for Nealtican lavas and Lorenzo pumice samples (data from Mangler et al., 2019). Red arrow represents the eruption progress and granodiorite data reported by Schaaf et al. (2005) (dark blue squares) and Mangler et al. (2019) (blue squares) are also plotted for comparison.

Atlimeyaya, etc.) as is documented here for the pre-Hispanic Tetimpa village.

Archaeological Impact and Future Volcanic Hazards

Historically in Mexico, significant damages have been associated with effusive volcanic activity. One example is Xitle volcano in the southern Mexico City Basin (Siebe, 2000), whose lavas buried in cal A.D. 250–530 the ancient towns of Cuicuilco (Fig. 1A) and Copilco, two pre-Classic sites. The pre-Classic or Formative refers to the period between 2500 B.C. and A.D. 200 in which the main features (e.g., agriculture based on corn, large-scale ceremonial architecture, etc.) of Mesoamerican culture initially developed (Vela, 2010). This eruption caused a great population exodus that surely generated a demographic and economic imbalance that favored the consolidation of Teotihuacan (Fig. 1A) as the main center of economic and political power in the northern part of the basin during the Classic period (Vela, 2009). A less important impact might be attributable to Chichinautzin volcano (Fig. 1), which erupted cal A.D. 65–350 and destroyed a considerable area at the southern margin of the Basin of Mexico (Siebe et al., 2004; Siebe and Macías, 2004).

A few hundred years earlier, the cal 350–50 B.C. Lorenzo Plinian eruption (VEI 6) deposited a >1-m-thick pumice fall on the lower eastern flank of the volcano, burying pre-Hispanic settlements (Siebe et al., 1996a; Panfil et al., 1999), such as Tetimpa (Seele, 1973; Plunket and Uruñuela, 1995, 1996, 1999, 2000, 2005, 2006). Shortly after the Plinian eruption, the massive Nealtican field buried part of the villages (Fig. 14) under 30–100 m of lava. Archaeological evidence indicates that shortly before these events, the population of the affected villages escaped either abruptly (Plunket and Uruñuela, 2009) or more gradually (Uruñuela and Plunket, 2003), which caused a temporary depopulation of this region. Uruñuela and Plunket (2003) suggest that during this period a few people frequently returned to protect possessions, but without inhabiting it. Plunket and Uruñuela (2000) found no evidence of human remains inside the collapsed dwellings where people might have sought refuge from the barrage of pumice. The emplacement of the Nealtican lavas may have been the final reason to mobilize people who refused to leave the region. The corridor that connected Teotihuacan with Puebla valley (Manzanilla, 2006) could have been used as a possible migration route. The Pedregal de Nealtican lava-flow field not only covered human settlements, but altered surface hydrology (Panfil et al., 1999), damming and diverting drainages (Fig. 14). At the base of the most distal flow fronts of unit F1, several springs occur near Atlimeyaya and Tianguismanalco (Fig. 2), some with considerable discharge (Fig. 14A). These waters flow beneath the lava along the former course of small paleo-creeks. Thus, the location of springs helps to reconstruct the drainage network before lava emplacement (Fig. 14B).

Siebe and Macías (2004) pointed out that it might not be a coincidence that the rise and fall of Teotihuacán (Sanders et al., 1979) and Cholula (Plunket and Uruñuela, 2000), the most important cities in central Mexico during the Classic period, defining Mesoamerican archaeology between A.D. 200 and 900, are bracketed by Popocatépetl's last major Plinian eruptions.

The Lorenzo Plinian eruption took place shortly before the first century A.D., when these cities were slowly emerging as the major urban hubs of the central plateau (Plunket and Uruñuela, 2000). Important contemporaneous late pre-Classic sites along the eastern edge of Popocatépetl volcano, like Colotzingo (Uruñuela, 1989), Coapa (Tschohl and Nickel, 1972), and Xochitécatl (Serra and Palavicini, 1996), show signs of abandonment (Fig. 1A). Plunket and Uruñuela (1998) suspect that these sites were largely abandoned after the volcanic disaster and that these groups nucleated as refugees in the city of Cholula. Similarly, between 100 B.C. and A.D. 100, settlements near Popocatépetl volcano in the southeastern part of the Basin of Mexico at the shores of Lake Chalco declined, while the

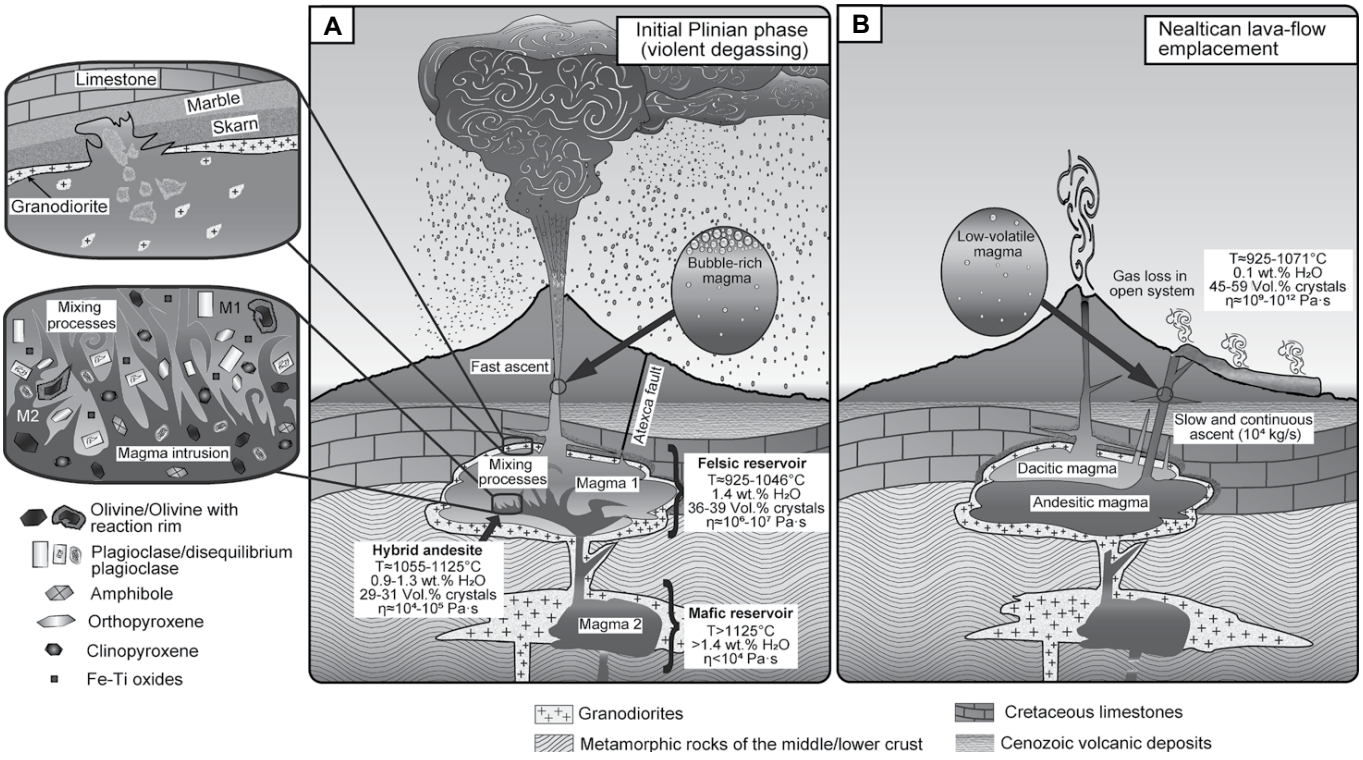

Figure 13. Schematic model of the Popocatépetl volcano in central Mexico depicting magma ascent through the crust, temporary storage in the upper crust, crystallization, and subsequent eruption. (A) Explosive phase of the cal 350–50 B.C. eruption, characterized by Plinian activity. A deep reservoir of mafic magma composition (Magma 2 (M2); with olivine, pyroxene, and amphibole) at ~8–17 km is in contact with granodiorite. A shallower reservoir of felsic magma composition (Magma 1 (M1); with plagioclase, ± pyroxene, and Fe-Ti oxides), at ~6 km is possibly hosted in limestone generating a contact aureole of skarn. The interaction between this reservoir and the limestones allows the incorporation of skarn and other xenoliths. At a given moment, the magma of the M2 reservoir reaches that of M1 and generates mixing processes that produce a hybrid andesitic composition. This interaction gives rise to the disequilibrium observed in the crystals and triggers the Lorenzo Plinian eruption due to the injection of volatiles into the magmatic chamber and a disequilibrium in the magmatic system. (B) Effusive phase eruption (Nealtican lava flows) characterized by efficient degassing of the magmatic system and a decrease in magma ascent and decompression rates. These lavas extrude along the Atexca fault. The less viscous andesitic magma propagates first through dikes, then the more viscous phenocryst-rich dacitic magma erupts.

Lake Zumpango and Teotihuacán Valley areas to the north of the basin gained substantially in population (Sanders et al., 1979).

Siebe (2000) and Plunket and Uruñuela (2006) propose that Popocatépetl's Lorenzo Plinian eruption is indirectly linked to Cuicuilco's downfall. The rise of Teotihuacan could well be a demographic and cultural consolidation in the late pre-Classic period, associated with the successive volcanic eruptions (of Popocatépetl and Xilte) at the southern margins of the Basin of Mexico that caused a massive exodus to Teotihuacan Valley to the north (Sanders et al., 1979; Siebe, 2000; Carballo and Pluckhan, 2007; Uruñuela and Plunket, 2007).

Despite risks of living near an active volcano, the eastern lower slopes of Popocatépetl became repopulated a few centuries after the Lorenzo cataclysmic eruption, perhaps for ritual reasons linked to the volcano, or because of the fertile land (Panfil et al., 1999). Since ancient times to the present, the Nealtican lavas have been quarried near the present towns of San Nicolás de los Ranchos and San Buenaventura Nealtican, Puebla, Mexico, for the handcrafted manufacture of domestic grinding tools (molcajetes and metates) and for building materials (Estrella et al., 2009). Today the extraction of andesite has intensified in numerous quarries along the lava flow margins, mainly as a construction and ornamental material. At these sites, workers occasionally discover archaeological remains beneath the lava. The eruption of such voluminous lavas, similar to the Nealtican lava field, poses a significant risk to communities' livelihoods in the periphery of Popocatépetl volcano. An event of this magnitude could destroy the infrastructure of entire towns and render agricultural areas permanently useless, as has occurred in the past.

CONCLUSIONS

This study provides new data to better understand effusive activity at Popocatépetl volcano. The geochemical, textural, and mineralogical evidence from the Nealtican lava-flow field (one of the most voluminous from Popocatépetl) points toward a magma-mixing processes at upper crustal levels, indicating that two separate magma batches mingled and/or mixed before final ascent and the gradual extrusion of lava flows. The magma-mixing preceded and triggered the explosive phase. Magma evolution during ascent through the crust was dominated by magma mixing, fractional crystallization, and minor assimilation. Nealtican rocks show abundant evidence of magmatic interaction with the basement and the upper crustal rocks. The stratigraphic relations of the Nealtican lavas and the Lorenzo Plinian pumice deposits indicate

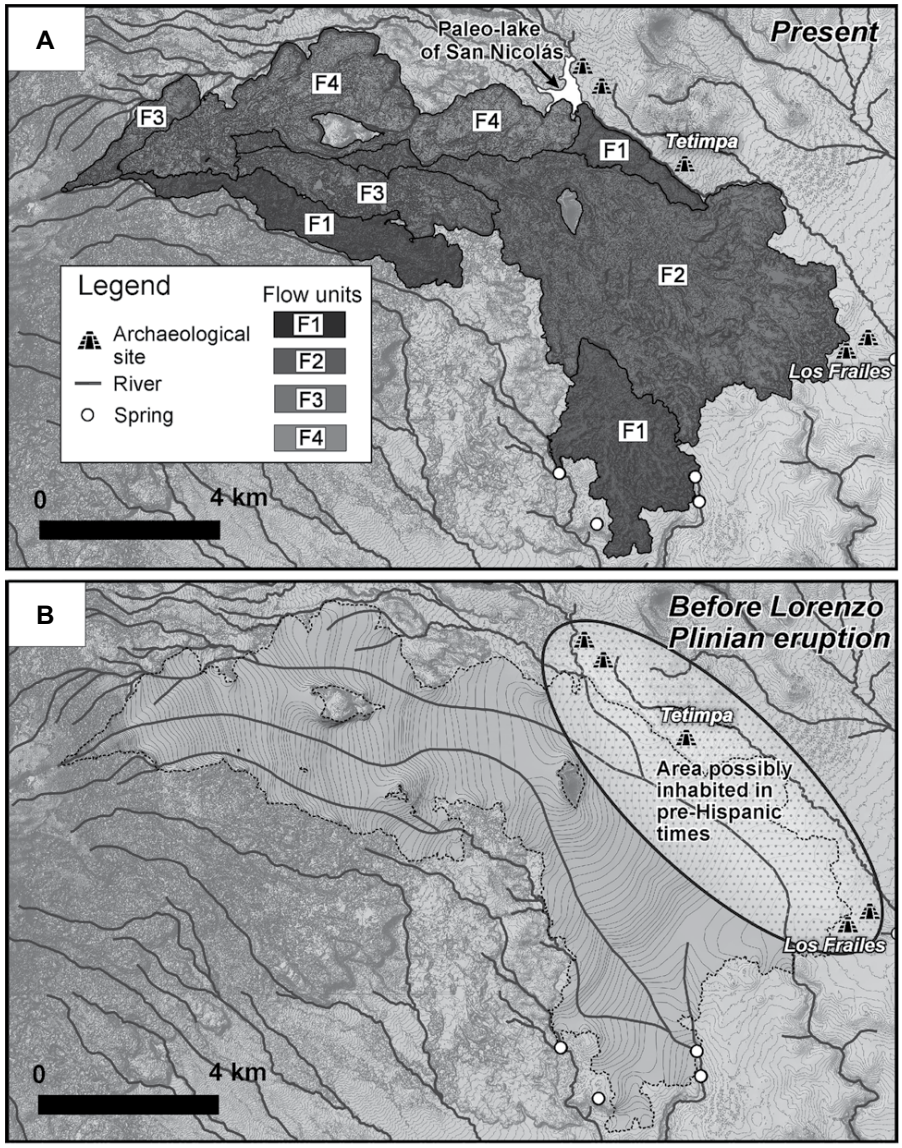

Figure 14. Hillshade-DEM of the Nealtican lava flows showing (A) present topography and flow units F1–F4, and (B) a simplified reconstruction of the topography before the cal 350–50 B.C. eruption. The drainage network after and before (inferred) the eruption, archaeological sites, and areas possibly inhabited in pre-Hispanic time but buried under the lava flows are also shown. Today several high-discharge springs are located at the most downvalley lava-flow.

that lava emplacement directly succeeded the explosive activity, maybe with a difference of months to years. The eruption dynamics changed from a Plinian to an effusive phase (Nealtican lava flows), a transition conditioned by decrease in the magma ascent and decompression rates linked to efficient degassing in an open system.

Magma viscosities (pre-eruptive conditions) were estimated at 10^4–10^7 Pa·s while lava viscosities during flow emplacement ranged between 10^9 and 10^{12} Pa·s. By analyzing the final dimensions of the lava flows, various models were used to estimate the eruption rates for two well-exposed lava flow units (F3 = ~0.65 km^3 and F4 = ~1.02 km^3). Estimated eruption rates range from 3 to 25 m^3/s and lava flow emplacement durations from 1 to 6 years for andesitic (unit F3), and from 1 to 13 m^3/s and 3–29 years for dacitic (unit F4) flows. The successive emplacement duration of all flows forming the Nealtican lava field (4.2 km^3) probably took 35 years (by a mean output rate of 15 m^3/s for andesitic lavas and of 1 m^3/s for dacitic lavas). The lava flows covered ~70 km^2 of terrain and put a final seal to the disastrous cal 350–50 B.C. Lorenzo Plinian eruption that temporarily depopulated this region in pre-Hispanic time.

This eruption, especially its initial Plinian phase, strongly affected human settlements around the volcano triggering migrations that had an impact on societies beyond this area. The present study could help define future eruptive scenarios and refine existing hazard analyses (e.g., Martin-Del Pozzo et al., 2017). The viscosity of such andesitic-dacitic flows is relatively high and their advancement velocity too slow to cause loss of human lives. Yet, such flows may destroy the infrastructure of entire towns and render agricultural areas permanently useless.

ACKNOWLEDGMENTS

Field and laboratory costs were defrayed by projects IN103618 and IN104221 granted to C. Siebe by the Dirección General de Asuntos del Personal Académico-Universidad Nacional Autónoma de México (UNAM). Israel Ramírez benefitted from a Consejo Nacional de Ciencia y Tecnología graduate-student fellowship (2017–2019). We thank Noemí Salazar and Giovanni Sosa for help with the electron-microprobe at Instituto de Geofísica, Unidad Michoacán, UNAM. Archaeologists Miguel Medina Jaen and Débora Lucía Muñoz Ribas (Instituto Nacional de Antropología e Historia de Mexico) provided useful information on the pre-Hispanic cultures of the study area. Lilia Arana Salinas and Fernando Ochoa Pérez are thanked for their support during fieldwork. John Ewert (Cascades Volcano Observatory, U.S. Geological Survey) kindly provided the photo used in Figure 1B. We thank Editor Brad S. Singer, Associate Editor Richard Waitt, and reviewers Valentin Troll and Brent Carr for their valuable suggestions that were very helpful in improving the original manuscript.

REFERENCES CITED

Aguilar-Murillo, C.A., 2012, Reconocimiento geológico de la zona de skarn de la Sierra de Tlayca y Tlayecac en el Estado de Morelos, México [B.A. thesis]: Hermosillo, México, Universidad de Sonora, 89 p.

Agustín-Flores, J., Siebe, C., and Guilbaud, M.N., 2011, Geology and geochemistry of Pelagatos, Cerro del Agua, and Dos Cerros monogenetic volcanoes in the Sierra Chichinautzin volcanic field, south of Mexico City: Journal of Volcanology and Geothermal Research, v. 201, p. 143–162, https://doi.org/10.1016/j.jvolgeores.2010.08.010.

Arámbula-Mendoza, R., Valdés-González, C., and Martínez-Bringas, A., 2010, Temporal and spatial variation of the stress state of Popocatépetl Volcano, Mexico: Journal of Volcanology and Geothermal Research, v. 196, p. 156–168, https://doi.org/10.1016/j.jvolgeores.2010.07.007.

Arana-Salinas, L., Siebe, C., and Macías, J.L., 2010, Dynamics of the ca. 4965 yr ^{14}C BP "Ochre Pumice" Plinian eruption of Popocatépetl volcano, México: Journal of Volcanology and Geothermal Research, v. 192, p. 212–231, https://doi.org/10.1016/j.jvolgeores.2010.02.022.

Atlas, Z.D., Dixon, J.E., Sen, G., Finny, M., and Martin-Del Pozzo, A.L., 2006, Melt inclusions from Volcan Popocatépetl and Volcan de Colima, Mexico: Melt evolution due to vapor-saturated crystallization during ascent: Journal of Volcanology and Geothermal Research, v. 153, p. 221–240, https://doi.org/10.1016/j.jvolgeores.2005.06.010.

Bachmann, O., and Bergantz, G.W., 2008, Rhyolites and their source mushes across tectonic settings: Journal of Petrology, v. 49, p. 2277–2285, https://doi.org/10.1093/petrology/egn068.

Beattie, P., 1993, Olivine-melt and orthopyroxene-melt equilibria: Contributions to Mineralogy and Petrology, v. 115, p. 103–111, https://doi.org/10.1007/BF00712982.

Cadoux, A., Missenard, Y., Martínez-Serrano, R.G., and Guillou, H., 2011, Trenchward Plio-Quaternary volcanism migration in the Trans-Mexican Volcanic Belt: The case of the Sierra Nevada range: Geological Magazine, v. 148, p. 492–506, https://doi.org/10.1017/S0016756810000993.

Campion, R., Delgado-Granados, H., Legrand, D., Taquet, N., Boulesteix, T., Pedraza-Espitía, S., and Lecocq, T., 2018, Breathing and coughing: The extraordinarily high degassing of Popocatépetl volcano investigated with an SO_2 camera: Frontiers of Earth Science, v. 6, p. 1–16, https://doi.org/10.3389/feart.2018.00163.

Capra, L., Macías, J.L., Scott, K.M., Abrams, M., and Garduño-Monroy, V.H., 2002, Debris avalanches and debris flows transformed from collapses in the Trans-Mexican volcanic belt, Mexico: Behavior, and implications for hazard assessment: Journal of Volcanology and Geothermal Research, v. 113, p. 81–110, https://doi.org/10.1016/S0377-0273(01)00252-9.

Carballo, D., and Pluckhan, T., 2007, Transportation corridors and political evolution in highland Mesoamerica: Settlement analyses incorporating GIS for northern Tlaxcala, Mexico: Journal of Anthropological Archaeology, v. 26, p. 607–629, https://doi.org/10.1016/j.jaa.2007.05.001.

Caricchi, L., Burlini, L., Ulmer, P., Gerya, T., Vassalli, M., and Papale, P., 2007, Non-Newtonian rheology of crystal-bearing magmas and implications for magma ascent dynamics: Earth and Planetary Science Letters, v. 264, p. 402–419, https://doi.org/10.1016/j.epsl.2007.09.032.

Carr, B.B., Clarke, A.B., Vanderkluysen, L., and Arrowsmith, J.R., 2019, Mechanisms of lava flow emplacement during an effusive eruption of Sinabung Volcano (Sumatra, Indonesia): Journal of Volcanology and Geothermal Research, v. 382, p. 137–148, https://doi.org/10.1016/j.jvolgeores.2018.03.002.

Cashman, K.V., 2004, Volatile controls on magma ascent and eruption, *in* Sparks, R.S.J., and Hawkesworth, C.J., eds., The State of the Planet: Frontiers and Challenges in Geophysics: Geophysical Monograph Series, v. 150, p. 109–124, https://doi.org/10.1029/150GM10.

Cassidy, M., Manga, M., and Cashman, K., 2018, Controls on explosive-effusive volcanic eruption styles: Nature Communications, v. 9, no. 2839, https://doi.org/10.1038/s41467-018-05293-3.

Castruccio, A., Rust, A.C., and Sparks, R.S.J., 2010, Rheology and flow of crystal-bearing lavas: Insights from analogue gravity currents: Earth and Planetary Science Letters, v. 297, p. 471–480, https://doi.org/10.1016/j.epsl.2010.06.051.

Castruccio, A., Rust, A.C., and Sparks, R.S.J., 2013, Evolution of crust- and core-dominated lava flows using scaling analysis: Bulletin of Volcanology, v. 75, p. 1–15, https://doi.org/10.1007/s00445-012-0681-2.

Chevrel, M.O., Platz, T., Hauber, E., Baratoux, D., Lavallée, Y., and Dingwell, D.B., 2013, Lava flow rheology: A comparison of morphological and petrological methods: Earth and Planetary Science Letters, v. 384, p. 109–120, https://doi.org/10.1016/j.epsl.2013.09.022.

Chevrel, M.O., Siebe, C., Guilbaud, M.N., and Salinas, S., 2016a, The AD 1250 El Metate shield volcano (Michoacán): Mexico's most voluminous Holocene eruption and its significance for archeology and hazards: The Holocene, v. 26, p. 471–488, https://doi.org/10.1177/0959683615609757.

Chevrel, M.O., Guilbaud, M.N., and Siebe, C., 2016b, The AD 1250 effusive eruption of El Metate shield volcano (Michoacán, Mexico): Magma source, crustal storage, eruptive dynamics, and lava rheology: Bulletin of Volcanology, v. 78, https://doi.org/10.1007/s00445-016-1020-9.

Chevrel, M.O., Pinkerton, H., and Harris, A.J.L., 2019, Measuring the viscosity of lava in the field: A review: Earth-Science Reviews, v. 196, p. 1–13, https://doi.org/10.1016/j.earscirev.2019.04.024.

Cimarelli, C., Costa, A., Mueller, S., and Mader, H.M., 2011, Rheology of magmas with bimodal crystal size and shape distributions: Insights from analog experiments: Geochemistry, Geophysics, Geosystems, v. 12, p. 1–14, https://doi.org/10.1029/2011GC003606.

Coombs, M.L., and Gardner, J.E., 2004, Reaction rim growth on olivine in silicic melts: implications for magma mixing: The American Mineralogist, v. 89, p. 748–758, https://doi.org/10.2138/am-2004-5-608.

Costa, A., Caricchi, L., and Bagdassarov, N., 2009, A model for the rheology of particle-bearing suspensions and partially molten rocks: Geochemistry, Geophysics, Geosystems, v. 10, p. 1525–1527, https://doi.org/10.1029/2008GC002138.

De Angelis, S.H., Larsen, J., Coombs, M., Dunn, A., and Hayden, L., 2015, Amphibole reaction rims as a record of pre-eruptive magmatic heating: An experimental approach: Earth and Planetary Science Letters, v. 426, p. 235–245, https://doi.org/10.1016/j.epsl.2015.06.051.

Deardorff, N.D., and Cashman, K.V., 2012, Emplacement conditions of the c. 1,600-year bp Collier Cone lava flow, Oregon: a LiDAR investigation: Bulletin of Volcanology, v. 74, p. 2051–2066, https://doi.org/10.1007/s00445-012-0650-9.

De la Cruz-Reyna, S., and Siebe, C., 1997, The giant Popocatépetl stirs: Nature, v. 388, no. 227 https://doi.org/10.1038/40749.

Del Gaudio, P., Ventura, G., and Taddeucci, J., 2013, The effect of particle size on the rheology of liquid-solid mixtures with application to lava flows: Results from analogue experiments: Geochemistry, Geophysics, Geosystems, v. 14, p. 2661–2669, https://doi.org/10.1002/ggge.20172.

De Silva, S.L., Self, S., Francis, P.W., Drake, R.E., and Ramirez, C.R., 1994, Effusive silicic volcanism in the Central Andes: The Chao dacite and other younger lavas of the Altiplanoe Puna Volcanic complex: Journal of Geophysical Research. Solid Earth, v. 99, p. 17805–17825, https://doi.org/10.1029/94JB00652.

Demant, A., 1978, Características del Eje Neovolcánico Transmexicano y sus problemas de interpretación: Revista Mexicana de Ciencias Geológicas, v. 2, p. 172–187.

DePaolo, D.J., 1981, Trace element and isotopic effects of combined wallrock assimilation and fractional crystallization: Earth and Planetary Science Letters, v. 53, p. 189–202, https://doi.org/10.1016/0012-821X(81)90153-9.

Dietterich, H.R., and Cashman, K.V., 2014, Channel networks within lava flows: Formation, evolution, and implications for flow behavior: Journal of Geophysical Research. Earth Surface, v. 119, p. 1704–1724, https://doi.org/10.1002/2014JF003103.

Dietterich, H.R., Downs, D.T., Stelten, M.E., and Zahran, H., 2018, Reconstructing lava flow emplacement histories with rheological and morphological analyses: The Harrat Rahat volcanic field, Kingdom of Saudi Arabia: Bulletin of Volcanology, v. 80, p. 1–23, https://doi.org/10.1007/s00445-018-1259-4.

Espinasa-Pereña, R., 2012, Historia de la actividad del volcán Popocatépetl, 17 años de erupciones: México, Centro Nacional de Prevencion de Desastres, 69 p.

Espinasa-Pereña, R., and Martin Del Pozzo, A.L., 2006, Morphostratigraphic evolution of Popocatépetl volcano, México, *in* Siebe, C., Macías, J.L., and Aguirre-Díaz, G.J., eds., Neogene-Quaternary Continental Margin Volcanism: A Perspective from Mexico: Geological Society of America, Special Papers, v. 402, p. 101–123, https://doi.org/10.1130/2006.2402(05).

Estrella, N., Morgado, A., Escudero, A.H., Abrego, H., Muñiz, I., Lima, J., Martínez, N., and Santos, R., 2009, Diagnóstico de la producción de artesanías en San Nicolás de los Ranchos: Las últimas manos que tallan la piedra, *in* Martínez, R., Rojo, G.E., Reyna, A., and Ramírez, B., eds., Diagnóstico Social Comunitario. Serie: Las Ciencias Sociales: México, Universidad Autónoma Indígena de México/Universidad Autónoma de Sinaloa/Colegio de Postgraduados-Puebla, p. 353–376.

Farquharson, J.I., James, M.R., and Tuffen, H., 2015, Examining rhyolite lava flow dynamics through photo-based 3D reconstructions of the 2011–2012 lava flow field at Cordón-Caulle, Chile: Journal of Volcanology and Geothermal Research, v. 304, p. 336–348, https://doi.org/10.1016/j.jvolgeores.2015.09.004.

Fink, J., 1980, Surface folding and viscosity of rhyolite flows: Geology, v. 8, p. 250–254, https://doi.org/10.1130/0091-7613(1980)8<250:SFAVOR>2.0.CO;2.

Fries, C., 1960, Geología del Estado de Morelos y partes adyacentes de México y Guerrero, región central meridional de México: Boletín del Instituto de Geología, Universidad Nacional Autónoma de México, v. 60, 236 p.

Fries, C., 1966, Hoja Cuernavaca 14Q-h(8): Resumen de la geología de la hoja Cuernavaca, Estados de Morelos, México, Guerrero y Puebla: México, Instituto de Geología, Universidad Nacional Autónoma de México, Carta Geológica de México, scale 1:100,000.

García-Tovar, G.P., and Martínez-Serrano, R.G., 2011, Geología y geoquímica de las lavas Pleistocénicas del estratovolcán Telapón, Sierra Nevada, México: Revista Mexicana de Ciencias Geológicas, v. 28, p. 301–322.

Geshi, N., Browning, J., and Kusumoto, S., 2020, Magmatic overpressures, volatile exsolution and potential explosivity of fissure eruptions inferred via dike aspect ratios: Scientific Reports, v. 10, p. 1–9, https://doi.org/10.1038/s41598-020-66226-z.

Ghiorso, M.S., and Evans, B.W., 2008, Thermodynamics of rhombohedral oxide solid solutions and a revision of the Fe-Ti two-oxide geothermometer and oxygen-barometer: American Journal of Science, v. 308, p. 957–1039, https://doi.org/10.2475/09.2008.01.

Gill, J.B., 1981, Orogenic Andesites and Plate Tectonics: New York, USA, Springer-Verlag, 390 p., https://doi.org/10.1007/978-3-642-68012-0.

Giordano, D., Russell, J.K., and Dingwell, D.B., 2008, Viscosity of magmatic liquids: A model: Earth and Planetary Science Letters, v. 271, p. 123–134, https://doi.org/10.1016/j.epsl.2008.03.038.

Goff, F., Janik, C.J., Delgado, H., Werner, C., Counce, D., Stimac, J.A., Siebe, C., Love, S.P., Williams, S.N., Fischer, T., and Johnson, L., 1998, Geochemical surveillance of magmatic volatiles at Popocatépetl volcano, México: Geological Society of America Bulletin, v. 110, p. 695–710, https://doi.org/10.1130/0016-7606(1998)110<0695:GSOMVA>2.3.CO;2.

Goff, F., Love, S.P., Warren, R.G., Counce, D., Obenholzner, J., Siebe, C., and Schmidt, S.C., 2001, Passive infrared remote sensing evidence for large, intermittent CO_2 emissions at Popocatépetl volcano, Mexico: Chemical Geology, v. 177, p. 133–156, https://doi.org/10.1016/S0009-2541(00)00387-9.

Gómez-Tuena, A., Orozco-Esquivel, M.T., and Ferrari, L., 2005, Petrogénesis ígnea de la Faja Volcánica Transmexicana: Boletín de la Sociedad Geológica Mexicana, v. 57, p. 227–283, https://doi.org/10.18268/BSGM-2005v57n3a2.

Gómez-Vazquez, A., De la Cruz-Reyna, S., and Mendoza-Rosas, A.T., 2016, The ongoing dome emplacement and destruction cyclic process at Popocatépetl volcano, Central Mexico: Bulletin of Volcanology, v. 78, no. 58, https://doi.org/10.1007/s00445-016-1054-z.

Gonnermann, H.M., and Manga, M., 2007, The fluid mechanics inside a volcano: Annual Review of Fluid Mechanics, v. 39, p. 321–356, https://doi.org/10.1146/annurev.fluid.39.050905.110207.

Griffiths, R.W., 2000, The dynamics of lava flows: Annual Review of Fluid Mechanics, v. 32, p. 477–518, https://doi.org/10.1146/annurev.fluid.32.1.477.

Griffiths, R.W., and Fink, J.H., 1993, Effects of surface cooling on the spreading of lava flows and domes: Journal of Fluid Mechanics, v. 252, p. 667–702, https://doi.org/10.1017/S0022112093003933.

Harris, A.J.L., Chevrel, M.O., Coppola, D., Ramsey, M.S., Hrysiewicz, A., Thivet, S., Villenueve, N., Favalli, M., Peltier, A., Kowalski, P., Di Muro, A., Froger, J.-L., and Gurioli, L. 2019, Validation of an integrated satellite-data-driven response to an effusive crisis: The April–May 2018 eruption of Piton de la Fournaise: Annals of Geophysics, v. 61, p. 1–18, https://doi.org/10.4401/ag-7972.

Harris, A.J.L., and Rowland, S.K., 2015, Lava flows and rheology, *in* Sigurdsson, H., ed., The Encyclopedia of Volcanoes: Cambridge, Massachusetts, USA, Academic Press, p. 321–342 https://doi.org/10.1016/B978-0-12-385938-9.00017-1.

Harris, A.J.L., Flynn, L.P., Matías, O., and Rose, W.I., 2002, The thermal stealth flows of Santiaguito dome, Guatemala: Implications for the cooling and emplacement of dacitic block-lava flows: Geological Society of America Bulletin, v. 114, p. 533–546, https://doi.org/10.1130/0016-7606(2002)114<0533:TTSFOS>2.0.CO;2.

Harris, A.J.L., Flynn, L.P., Matias, O., Rose, W.I., and Cornejo, J., 2004, The evolution of an active silicic lava flow field: an ETM+ perspective: Journal of Volcanology and Geothermal Research, v. 135, p. 147–168, https://doi.org/10.1016/j.jvolgeores.2003.12.011.

Hawkesworth, C.J., O'nions, R.K., Pankhurst, R.J., Hamilton, P.J., and Evensen, N.M., 1977, A geochemical study of island-arc and back-arc tholeiites from the Scotia Sea: Earth and Planetary Science Letters, v. 36, p. 253–262, https://doi.org/10.1016/0012-821X(77)90207-2.

Hulme, G., 1974, The interpretation of lava flow morphology: Geophysical Journal of the Royal Astronomical Society, v. 39, p. 361–383, https://doi.org/10.1111/j.1365-246X.1974.tb05460.x.

Hulme, G., and Fielder, G., 1977, Effusion rates and rheology of lunar lavas: Philosophical Transactions of the Royal Society of London. Series A, Mathematical and Physical Sciences, v. 285, p. 227–234, https://doi.org/10.1098/rsta.1977.0059.

Irvine, T.N., and Baragar, W.R.A., 1971, A guide to the chemical classification of the common volcanic rocks: Canadian Journal of Earth Sciences, v. 8, p. 523–548, https://doi.org/10.1139/e71-055.

Jeffreys, H., 1925, The flow of water in an inclined channel of rectangular section: The London, Edinburgh and Dublin Philosophical Magazine and Journal of Science, v. 49, p. 793–807, https://doi.org/10.1080/14786442508634662.

Jolis, E.M., Troll, V.R., Harris, C., Freda, C., Gaeta, M., Orsi, G., and Siebe, C., 2015, Skarn xenolith record crustal CO_2 liberation during Pompeii and Pollena eruptions, Vesuvius volcanic system, central Italy: Chemical Geology, v. 415, p. 17–36, https://doi.org/10.1016/j.chemgeo.2015.09.003.

Kerr, R.C., and Lyman, A.W., 2007, Importance of surface crust strength during the flow of the 1988–1990 andesite lava of Lonquimay Volcano, Chile: Journal of Geophysical Research. Solid Earth, v. 112, p. 1–8, https://doi.org/10.1029/2006JB004522.

Kerr, R.C., Griffiths, R.W., and Cashman, K.V., 2006, Formation of channelized lava flows on an unconfined slope: Journal of Geophysical Research. Solid Earth, v. 111, p. 1–13, https://doi.org/10.1029/2005JB004225.

Kilburn, C.R.J., and Lopes, R., 1991, General patterns of flow field growth: Aa and blocky lavas: Journal of Geophysical Research. Solid Earth, v. 96, p. 19721–19732, https://doi.org/10.1029/91JB01924.

Kolisnik, A.M.E., 1990, Phenocryst zoning, and heterogeneity in andesite and dacite of Volcan Popocatépetl, Mexico [M.S. thesis]: Kingston, Ontario, Canada, Queen's University, 247 p.

Larocque, A.C.L., Stimac, J.A., and Siebe, C., 1998, Metal-residence sites in lavas and tuffs from Volcán Popocatepetl, Mexico: Implications for metal mobility in the environment: Environmental Geology, v. 33, p. 197–208, https://doi.org/10.1007/s002540050238.

Larrea, P., Salinas, S., Widom, E., Siebe, C., and Abbitt, R.J.F., 2017, Compositional and volumetric development of a monogenetic lava flow field: The historical case of Paricutin (Michoacán, Mexico): Journal of Volcanology and Geothermal Research, v. 348, p. 36–48, https://doi.org/10.1016/j.jvolgeores.2017.10.016.

Larrea, P., Widom, E., Siebe, C., Salinas, S., and Kuentz, D., 2019, A re-interpretation of the petrogenesis of Paricutin volcano: Distinguishing crustal contamination from mantle heterogeneity: Chemical Geology, v. 504, p. 66–82, https://doi.org/10.1016/j.chemgeo.2018.10.026.

Latutrie, B., Harris, A., Médard, E., and Gurioli, L., 2017, Eruption and emplacement dynamics of a thick trachytic lava flow of the Sancy volcano (France): Bulletin of Volcanology, v. 79, p. 1–21, https://doi.org/10.1007/s00445-016-1084-6.

Lavallée, Y., Hess, K.U., Cordonnier, B., and Dingwell, D.B., 2007, Non-Newtonian rheological law for highly crystalline dome lavas: Geology, v. 35, p. 843–846, https://doi.org/10.1130/G23594A.1.

Le Bas, M.J., Le Maitre, R.W., Streckeisen, A., and Zanettin, B., 1986, A chemical classification of volcanic rocks based on the total alkali-silica diagram: Journal of Petrology, v. 27, p. 745–750, https://doi.org/10.1093/petrology/27.3.745.

Lefler, E., 2011, Genauigkeitsbetrachtung bei der Ermittlung rheologischer Parameter von Lavaströmen aus Fernerkundungsdaten [B.A. thesis]: Berlin, Germany, Free University of Berlin, 68 p.

Love, S.P., Goff, F., Counce, D., Siebe, C., and Delgado, H., 1998, Passive infrared spectroscopy of the eruption plume at Popocatépetl volcano, México: Nature, v. 396, p. 563–567, https://doi.org/10.1038/25109.

Luhr, J.F., and Carmichael, I.S.E., 1982, The Colima Volcanic Complex, Mexico. III. Ash- and scoria-fall deposits from the upper slopes of Volcán Colima: Contributions to Mineralogy and Petrology, v. 80, p. 262–275, https://doi.org/10.1007/BF00371356.

Macías, J.L., and Siebe, C., 2005, Popocatépetl's crater filled to the brim: Significance for hazard evaluation: Journal of Volcanology and Geothermal Research, v. 141, p. 327–330, https://doi.org/10.1016/j.jvolgeores.2004.10.005.

Macías, J.L., Carrasco, G., Delgado, H., Martin Del Pozzo, A.L., Siebe, C., Hoblitt, R., Sheridan, M.F., and Tilling, R.I., 1995, Mapa de peligros volcánicos del Popocatépetl: Mexico, Publicación Especial del Instituto de Geofísica, Universidad Nacional Autónoma de México.

Macías, J.L., Arce, J.L., García-Tenorio, F., Layer, P.W., Rueda, H., Reyes-Agustín, G., López-Pizaña, F., and Avellán, D., 2012, Geology and geochronology of Tláloc, Telapón, Iztaccíhuatl, and Popocatépetl volcanoes, Sierra Nevada, central Mexico: Geological Society of America Field Guide, v. 25, p. 163–193, https://doi.org/10.1130/2012.0025(08).

Macías, J.L., Arce, J.L., García-Tenorio, F., Sosa-Ceballos, G., and Gardner, J.E., 2020, Source and behavior of pyroclastic density currents generated by Vulcanian-style explosions of Popocatépetl volcano (Mexico) on 22 January 2001: Journal of Volcanology and Geothermal Research, v. 406, https://doi.org/10.1016/j.jvolgeores.2020.107071.

Magnall, N., James, M.R., Tuffen, H., and Vye-Brown, C., 2017, Emplacing a cooling-limited rhyolite lava flow: Similarities with basaltic lava flows: Frontiers of Earth Science, v. 5, p. 1–19, https://doi.org/10.3389/feart.2017.00044.

Magnall, N., James, M.R., Tuffen, H., Vye-Brown, C., Schipper, C.I., Castro, J.M., and Davies, A.G., 2019, The origin and evolution of breakouts in a cooling-limited rhyolite lava flow: Geological Society of America Bulletin, v. 131, p. 137–154, https://doi.org/10.1130/B31931.1.

Mangler, M., Prytulak, J., Gisbert, G., Delgado-Granados, H., and Petrone, C., 2019, Interplinian effusive activity at Popocatépetl volcano, Mexico: New insights into evolution and dynamics of the plumbing system: Volcanica, v. 2, p. 45–72, https://doi.org/10.30909/vol.02.01.4572.

Manzanilla, L., 2006, Estados corporativos arcaicos: Organizaciones de excepción en escenarios excluyentes: Cuicuilco, v. 13, p. 13–15.

Mares-Tepanohaya, R.U., 2014, Caracterización geoquímica y gemológica de los granates del skarn de la Sierra de Tlayca, Morelos [B.A thesis]: Ciudad de México, México, Universidad Nacional Autónoma de México, 71 p.

Martin Del Pozzo, A.L., Alatorre Ibargüengoitia, M., Arana Salinas, L., Bonasia, R., Capra Pedol, L., Cassata, W., Córdoba, G., Cortés Ramos, J., Delgado Granados, H., Ferrés López, M.D., Fonseca Álvarez, R., García Reynoso, J.A., Gisbert, G., Guerrero López, D.A., Jaimes Viera, M.C., Macías Vázquez, J.L., Nieto Obregón, J., Nieto Torres, A., Paredes Ruiz, P.A., Portocarrero Martínez, J., Renne, P., Rodríguez Espinosa, D.M., Salinas Sánchez, S., Siebe Grabach, C., and Tellez Ugalde, E., 2017, Estudios geológicos y actualización del mapa de peligros del volcán Popocatépetl: Memoria técnica del mapa de peligros del volcán Popocatépetl: Monografías del Instituto de Geofísica, Universidad Nacional Autónoma de México, 160 p.

McDonough, W.F., and Sun, S.S., 1995, The composition of the Earth: Chemical Geology, v. 120, p. 223–253, https://doi.org/10.1016/0009-2541(94)00140-4.

Mendoza-Rosas, A.T., Gómez-Vázquez, A., and De la Cruz-Reyna, S., 2017, Statistical analysis of the sustained lava dome emplacement and destruction processes at Popocatépetl volcano, Central México: Bulletin of Volcanology, v. 79, no. 43, https://doi.org/10.1007/s00445-017-1127-7.

Microsoft Bing Map, 2019, Landsat Satellite Images of Earth by Earthstar Geographics: https://www.bing.com/maps/ (accessed January 2019).

Morimoto, N., 1988, Nomenclature of Pyroxenes: Mineralogy and Petrology, v. 39, p. 55–76, https://doi.org/10.1007/BF01226262.

Nakada, S., and Motomura, Y., 1999, Petrology of the 1991–1995 eruption at Unzen: Effusion pulsation and groundmass crystallization: Journal of Volcanology and Geothermal Research, v. 89, p. 173–196, https://doi.org/10.1016/S0377-0273(98)00131-0.

Naranjo, J.A., Sparks, R.S.J., Stasiuk, M.V., Moreno, H., and Ablay, G.J., 1992, Morphological, structural and textural variations in the 1988–1990 andesite lava of Lonquimay Volcano, Chile: Geological Magazine, v. 129, p. 657–678, https://doi.org/10.1017/S0016756800008426.

Navarro-Ochoa, C., Gavilanes-Ruiz, J.C., and Cortes-Cortes, A., 2002, Movement and emplacement of lava flows at Volcan de Colima, Mexico: November 1998–February 1999: Journal of Volcanology and Geothermal Research, v. 117, p. 155–167, https://doi.org/10.1016/S0377-0273(02)00242-1.

Nelson, S., 1980, Geology and petrology of Volcán Ceboruco, Nayarit, México: Geological Society of America Bulletin, v. 91, p. 2290–2431, https://doi.org/10.1130/GSAB-P2-91-2290.

Nguyen, C.T., Gonnermann, H.M., and Houghton, B.F., 2014, Explosive to effusive transition during the largest volcanic eruption of the 20th century (Novarupta 1912, Alaska): Geology, v. 42, p. 703–706, https://doi.org/10.1130/G35593.1.

Nichols, R.L., 1939, Viscosity of lava: The Journal of Geology, v. 47, p. 290–302, https://doi.org/10.1086/624778.

Nixon, G., 1982, The relationship between Quaternary volcanism in central Mexico and the seismicity and structure of subducted ocean lithosphere: Geological Society of America Bulletin, v. 93, p. 514–523, https://doi.org/10.1130/0016-7606(1982)93<514:TRBQVI>2.0.CO;2.

Nixon, G., 1988a, Petrology of the younger andesites and dacites of Iztaccíhuatl volcano, México: I. Disequilibrium phenocrysts assemblages as indicators of magma chamber processes: Journal of Petrology, v. 29, p. 213–264, https://doi.org/10.1093/petrology/29.2.213.

Nixon, G., 1988b, Petrology of the younger andesites and dacites of Iztaccíhuatl volcano, México: II. Chemical stratigraphy, magma mixing, and the composition of basaltic magma influx: Journal of Petrology, v. 29, p. 265–303, https://doi.org/10.1093/petrology/29.2.265.

Pallister, J., Wessels, R., Griswold, J., McCausland, W., Kartadinata, N., Gunawan, H., Budianto, A., and Primulyana, S., 2019, Monitoring, forecasting collapse events, and mapping pyroclastic deposits at Sinabung volcano with satellite imagery: Journal of Volcanology and Geothermal Research, v. 382, p. 149–163, https://doi.org/10.1016/j.jvolgeores.2018.05.012.

Panfil, M.S., Gardner, T.W., and Hirth, K.G., 1999, Late Holocene stratigraphy of the Tetimpa archaeological sites, northeast flank of Popocatépetl volcano, Central Mexico: Geological Society of America Bulletin, v. 111, p. 204–218, https://doi.org/10.1130/0016-7606(1999)111<0204:LHSOTT>2.3.CO;2.

Pardo, M., and Suárez, G., 1995, Shape of the subducted Rivera and Cocos plates in southern Mexico: Seismic and tectonic implications: Journal of Geophysical Research. Solid Earth, v. 100, p. 12357–12373, https://doi.org/10.1029/95JB00919.

Peters, S.T., Troll, V.R., Weis, F.A., Dallai, L., Chadwick, J.P., and Schulz, B., 2017, Amphibole megacrysts as a probe into the deep plumbing system of Merapi volcano, Central Java, Indonesia: Contributions to Mineralogy and Petrology, v. 172, p. 1–20, https://doi.org/10.1007/s00410-017-1338-0.

Pinkerton, H., 1987, Factor affecting the morphology of lava flows: Endeavour, v. 11, p. 73–79, https://doi.org/10.1016/0160-9327(87)90241-9.

Pinkerton, H., and Sparks, R.S.J., 1976, The 1975 sub-terminal lavas, Mount Etna: A case history of the formation of a compound lava field: Journal of Volcanology and Geothermal Research, v. 1, p. 167–182, https://doi.org/10.1016/0377-0273(76)90005-6.

Pinkerton, H., and Wilson, L., 1994, Factor controlling the lengths of channel-fed lava flows: Bulletin of Volcanology, v. 56, p. 108–120, https://doi.org/10.1007/BF00304106.

Pioli, L., Azzopardi, B.J., and Cashman, K.V., 2009, Controls on the explosivity of scoria cone eruptions: Magma segregation at conduit junctions: Journal of Volcanology and Geothermal Research, v. 186, p. 407–415, https://doi.org/10.1016/j.jvolgeores.2009.07.014.

Pistone, M., Caricchi, L., Ulmer, P., Burlini, L., Ardia, P., Reusser, E., Marone, F., and Arbaret, L., 2012, Deformation experiments of bubble- and crystal-bearing magmas: Rheological and microstructural analysis: Journal of Geophysical Research. Solid Earth, v. 117, p. 1–39, https://doi.org/10.1029/2011JB008986.

Pistone, M., Cordonnier, B., Ulmer, P., and Caricchi, L., 2016, Rheological flow laws for multiphase magmas: An empirical approach: Journal of Volcanology and Geothermal Research, v. 321, p. 158–170, https://doi.org/10.1016/j.jvolgeores.2016.04.029.

Plunket, P., and Uruñuela, G., 1995, Proyecto Tetimpa: Informe técnico al Consejo de Arqueología, Instituto Nacional de Antropología e Historia, primera temporada: Puebla, México, Universidad de las Américas, 161 p.

Plunket, P., and Uruñuela, G., 1996, Las Unidades Domésticas de Tetimpa: XXIV Mesa Redonda de la Sociedad Mexicana de Antropología, Tepic, Nayarit, México, v. 3, p. 1841–1857.

Plunket, P., and Uruñuela, G., 1998, Preclassic household patterns preserved under volcanic ash at Tetimpa, Puebla, Mexico: Latin American Antiquity, v. 9, p. 287–309, https://doi.org/10.2307/3537029.

Plunket, P., and Uruñuela, G., 1999, Pueblos sin memoria: Lecciones del Popocatépetl: Cuicuilco, v. 5, p. 11–25.

Plunket, P., and Uruñuela, G., 2000, The quick and the dead: Decision making during the abandonment of Tetimpa: Mayab, v. 13, p. 78–87.

Plunket, P., and Uruñuela, G., 2005, Recent research in Puebla prehistory: Journal of Archaeological Research, v. 13, p. 89–127, https://doi.org/10.1007/s10804-005-2485-5.

Plunket, P., and Uruñuela, G., 2006, Social and cultural consequences of a late Holocene eruption of Popocatépetl in central Mexico: Quaternary International, v. 151, p. 19–28, https://doi.org/10.1016/j.quaint.2006.01.012.

Plunket, G., and Uruñuela, P., 2009, El Popocatépetl y la legendaria lluvia de fuego, *in* Vela, E., ed., Los Volcanes de México: Arqueología Mexicana, v. 16, p. 59–63.

Putirka, K., 2005, Igneous thermometers and barometers based on plagioclase + liquid equilibria: tests of some existing models and new calibrations: The American Mineralogist, v. 90, p. 336–346, https://doi.org/10.2138/am.2005.1449.

Putirka, K.D., 2008, Thermometers and barometers for volcanic systems: Reviews in Mineralogy and Geochemistry, v. 69, p. 61–120, https://doi.org/10.2138/rmg.2008.69.3.

Putirka, K., Johnson, M., Kinzler, R., and Walker, D., 1996, Thermobarometry of mafic igneous rocks based on clinopyroxene-liquid equilibria, 0–30 kbar: Contributions to Mineralogy and Petrology, v. 123, p. 92–108, https://doi.org/10.1007/s004100050145.

Putirka, K., Ryerson, F.J., and Mikaelian, H., 2003, New igneous thermobarometers for mafic and evolved lava compositions, based on clinopyroxene + liquid equilibria: The American Mineralogist, v. 88, p. 1542–1554, https://doi.org/10.2138/am-2003-1017.

Ramírez-Uribe, I., Siebe, C., Chevrel, M.O., and Fisher, C.T., 2021, Rancho Seco monogenetic volcano (Michoacán, Mexico): Petrogenesis and lava flow emplacement based on LiDAR images: Journal of Volcanology and Geothermal Research, v. 411, p. 1–19, https://doi.org/10.1016/j.jvolgeores.2020.107169.

Reyes-Guzmán, N., Siebe, C., Chevrel, M.O., and Pereira, G., 2021, Late Holocene Malpaís de Zacapu (Michoacán, Mexico) lava flows: Rheology and eruption durations from LiDAR high-resolution topography and mineral-equilibrium temperature estimates: Bulletin of Volcanology, v. 83, p. 1–21, https://doi.org/10.1007/s00445-021-01449-0.

Roberge, J., Delgado-Granados, H., and Wallace, P.J., 2009, Mafic magma recharge supplies high CO_2 and SO_2 gas fluxes from Popocatépetl volcano, Mexico: Geology, v. 37, p. 107–110, https://doi.org/10.1130/G25242A.1.

Robert, B., Harris, A., Gurioli, G., Medard, E., Sehlke, A., and Whittington, A., 2014, Textural and rheological evolution of basalt flowing down a lava channel: Bulletin of Volcanology, v. 76, p. 1–21, https://doi.org/10.1007/s00445-014-0824-8.

Robin, C., 1984, Le volcan Popocatépetl (Mexique): Structure, evolution pétrologique et risques: Bulletin of Volcanology, v. 47, p. 1–23, https://doi.org/10.1007/BF01960537.

Robin, C., Camus, G., and Gourgaud, A., 1991, Eruptive and magmatic cycles at Fuego de Colima volcano (México): Journal of Volcanology and Geothermal Research, v. 45, p. 209–225, https://doi.org/10.1016/0377-0273(91)90060-D.

Rudnick, R.L., and Gao, S., 2003, Composition of the continental crust, *in* Rudnick, R.L., Holland, H.D., and Turekian, K.K., eds., Treatise on Geochemistry-The Crust: Oxford, UK, Elsevier, v. 3, p. 1–64, https://doi.org/10.1016/B0-08-043751-6/03016-4.

Rutherford, M.J., 2008, Magma ascent rates: Reviews in Mineralogy and Geochemistry, v. 69, p. 241–271, https://doi.org/10.2138/rmg.2008.69.7.

Rutherford, M.J., and Hill, P.M., 1993, Magma ascent rates from amphibole breakdown: An experimental study applied to the 1980–1986 Mount St. Helens eruptions: Journal of Geophysical Research. Solid Earth, v. 98, p. 19667–19685, https://doi.org/10.1029/93JB01613.

Sanders, W.T., Parsons, J., and Santley, R.S., 1979, The Basin of Mexico: Ecological processes in the evolution of a civilization: American Antiquity, v. 45, p. 843–886, https://doi.org/10.2307/280159.

Schaaf, P., Stimac, J., Siebe, C., and Macías, J., 2005, Geochemical evidence for mantle origin and crustal processes in volcanic rocks from Popocatépetl and surrounding monogenetic volcanoes, central Mexico: Journal of Petrology, v. 46, p. 1243–1282, https://doi.org/10.1093/petrology/egi015.

Seele, E., 1973, Restos de Milpas y poblaciones prehispánicas cerca de San Juan Buenaventura Nealtican, Puebla: Comunicaciones, v. 7, p. 77–86.

Serra, M.C., and Palavicini, B., 1996, Xochitécatl, Tlaxcala, en el Periodo Formativo (800 a.C.-100 d.C.): Arqueología, v. 16, p. 149–157.

Sheridan, M.F., Hubbard, B., Bursik, M.I., Siebe, C., Abrams, M., Macías, J.L., and Delgado, G.H., 2001, Gauging short-term volcanic hazards at Popocatépetl: Eos (Washington, D.C.), v. 82, p. 185–188, https://doi.org/10.1029/01EO00097.

Siebe, C., 2000, Age and archaeological implications of Xitle volcano, southwestern basin of Mexico-City: Journal of Volcanology and Geothermal Research, v. 104, p. 45–64, https://doi.org/10.1016/S0377-0273(00)00199-2.

Siebe, C., and Macías, J.L., 2004, Volcanic hazards in the Mexico City metropolitan area from eruptions at Popocatépetl, Nevado de Toluca, and Jocotitlán stratovolcanoes and monogenetic scoria cones in the Sierra Chichinautzin Volcanic Field, *in* Siebe, C., Macías, J.L., and Aguirre, G., eds., Neogene-Quaternary Continental Margin Volcanism: A Perspective From Mexico: Geological Society of America, Special Papers, v. 402, p. 253–329.

Siebe, C., Abrams, M., and Macías, J.L., 1995, Derrumbes gigantes, depósitos de avalancha de escombros y edad del actual cono del volcán Popocatépetl: Volcán Popocatépetl, estudios realizados durante la crisis de 1994–1995: México, Centro Nacional de Prevencion de Desastres, p. 195–220.

Siebe, C., Abrams, M., Macías, J.L., and Obenholzner, J.H., 1996a, Repeated volcanic disasters in prehispanic time at Popocatepetl, Central Mexico: Past key to the future?: Geology, v. 24, p. 399–402, https://doi.org/10.1130/0091-7613(1996)024<0399:RVDIPT>2.3.CO;2.

Siebe, C., Macías, J.L., Abrams, M., and Obenholzner, J., 1996b, La destrucción de Cacaxtla y Cholula: Un suceso en la historia eruptiva del Popocatépetl: Revista Ciencias, Universidad Nacional Autónoma de México, v. 43, p. 36–45.

Siebe, C., Rodríguez-Lara, V., Schaaf, P., and Abrams, M., 2004, Radiocarbon ages of Holocene Pelado, Guespalapa, and Chichinautzin scoria cones, south of Mexico-City: Implications for archaeology and future hazards: Bulletin of Volcanology, v. 66, p. 203–225, https://doi.org/10.1007/s00445-003-0304-z.

Siebe, C., Salinas, S., Arana-Salinas, L., Macías, J.L., Gardner, J., and Bonasia, R., 2017, The ∼23,500 y ^{14}C BP White Pumice Plinian eruption and associated debris avalanche and Tochimilco lava flow of Popocatépetl volcano, México: Journal of Volcanology and Geothermal Research, v. 333–334, p. 66–95, https://doi.org/10.1016/j.jvolgeores.2017.01.011.

Sosa-Ceballos, G., Gardner, J., Siebe, C., and Macías, J.L., 2012, A caldera-forming eruption ∼14,100 ^{14}C yr BP at Popocatépetl volcano, México: Insights from eruption dynamics and magma mixing: Journal of Volcanology and Geothermal Research, v. 213–214, p. 27–40, https://doi.org/10.1016/j.jvolgeores.2011.11.001.

Sosa-Ceballos, G., Gardner, J., and Lassiter, J.C., 2014, Intermittent mixing processes occurring before Plinian eruptions of Popocatépetl volcano, Mexico: Insights from textural and compositional variations in plagioclase and Sr-Nd-Pb isotopes: Contributions to Mineralogy and Petrology, v. 167, p. 1–19, https://doi.org/10.1007/s00410-014-0966-x.

Sosa-Ceballos, G., Macías, J.L., García-Tenorio, F., Layer, P., Schaaf, P., Solís-Pichardo, G., and Arce, J.L., 2015, El Ventorrillo, a paleostructure of Popocatépetl volcano: Insights from geochronology and geochemistry: Bulletin of Volcanology, v. 77, p. 1–20, https://doi.org/10.1007/s00445-015-0975-2.

Sparks, S., Sigurdsson, H., and Wilson, L., 1977, Magma mixing: A mechanism for triggering acid explosive eruptions: Nature, v. 267, p. 315–318, https://doi.org/10.1038/267315a0.

Straub, S., and Martín-Del Pozzo, A., 2001, The significance of phenocryst diversity in tephra from recent eruptions at Popocatépetl Stratovolcano (central Mexico): Contributions to Mineralogy and Petrology, v. 140, p. 487–510, https://doi.org/10.1007/PL00007675.

Stremme, W., Ortega, I., Siebe, C., and Grutter, M., 2011, Gas composition of Popocatépetl volcano between 2007 and 2008: FTIR spectroscopic measurements of an explosive event and during quiescent degassing: Earth and Planetary Science Letters, v. 301, p. 502–510, https://doi.org/10.1016/j.epsl.2010.11.032.

Stuiver, M., Reimer, P.J., and Reimer, R.W., 2021, CALIB ^{14}C Calibration Program Version 8.2: http://calib.org (accessed September 2021).

Sun, S.S., and McDonough, W.F., 1989, Chemical and isotopic systematics of oceanic basalts: Implications for mantle composition and processes, *in* Saunders, A.D., and Norry, M.J., eds., Magmatism in the Ocean Basins: Geological Society of London, Special Publications, v. 42, p. 313–345, https://doi.org/10.1144/GSL.SP.1989.042.01.19.

Takeuchi, S., 2011, Preeruptive magma viscosity: An important measure of magma eruptibility: Chemistry and Physics of Minerals and Rocks/Volcanology, v. 116, p. 1–19, https://doi.org/10.1029/2011JB008243.

Taquet, N., Stremme, W., Grutter, M., Baylón, J., Bezanilla, A., Schiavo, B., Rivera, C., Campion, R., Boulesteix, T., Nieto-Torres, A., Espinasa-Pereña, R., Blumenstock, T., and Hase, F., 2019, Variability in the gas composition of the Popocatepetl volcanic plume: Frontiers of Earth Science, v. 7, p. 1–14, https://doi.org/10.3389/feart.2019.00114.

Torres-Orozco, R., Arce, J.L., Layer, P.W., and Benowitz, J.A., 2017, The Quaternary history of effusive volcanism of the Nevado de Toluca area, central Mexico: Journal of South American Earth Sciences, v. 79, p. 12–39, https://doi.org/10.1016/j.jsames.2017.07.008.

Tschohl, P., and Nickel, H., 1972, Catálogo arqueológico y etnohistórico de Puebla-Tlaxcala, México: Mexico, Fundación Alemana para la Investigación Científica, v. 1, 573 p.

Tuffen, H., James, M.R., Castro, J.M., and Schipper, C.I., 2013, Exceptional mobility of an advancing rhyolitic

obsidian flow at Cordon Caulle volcano in Chile: Nature Communications, v. 4, p. 1–7, https://doi.org/10.1038/ncomms3709.

Ueki, K., Inui, M., Matsunaga, K., Okamoto, N., and Oshio, K., 2020, Oxidation during magma mixing recorded by symplectites at Kusatsu–Shirane Volcano, Central Japan: Earth, Planets and Space, v. 72, p. 1–12, https://doi.org/10.1186/s40623-020-01192-4.

Uruñuela, G., 1989, Investigaciones arqueológicas en Colotzingo, Puebla: Notas Mesoamericanas, v. 11, p. 110–119.

Uruñuela, G., and Plunket, P., 2003, Testimonios de diversos tipos de abandono en Tetimpa, Puebla: Trace (México, D.F.), v. 43, p. 84–96, https://doi.org/10.22134/trace.43.2003.526.

Uruñuela, G., and Plunket, P., 2007, Tradition and transformation: Village ritual at Tetimpa as a template for early Teotihuacan, *in* Gonlin, N., and Lohse, J.C., eds., Commoner Ritual and Ideology in Ancient Mesoamerica: Boulder, Colorado, University Press of Colorado, p. 33–54.

Vela, E., 2009, Los volcanes de México: Arqueología Mexicana, v. 16, p. 1–88.

Vela, E., 2010, Preclásico (2500 a.C.-200 d.C.), *in* Vela, E., ed., Culturas Prehispánicas: Arqueología Mexicana, v. 34, p. 15–21.

Vicari, A., Bilotta, G., Bonfiglio, S., Cappello, A., Ganci, G., Hérault, A., Rustico, E., Gallo, G., and Del Negro, C., 2011, LAV@Hazard: A web-GIS interface for volcanic hazard assessment: Annals of Geophysics, v. 54, p. 662–670, https://doi.org/10.4401/ag-5347.

Walker, G.P.L., 1973, Lengths of lava flows: Philosophical Transactions of the Royal Society, v. 274, p. 107–118.

Waters, L.E., and Lange, R.A., 2015, An updated calibration of the plagioclase-liquid hygrometer-thermometer applicable to basalts through rhyolites: The American Mineralogist, v. 100, p. 2172–2184, https://doi.org/10.2138/am-2015-5232.

Watts, R.B., Herd, R.A., Sparks, R.S.J., and Young, S.R., 2002, Growth patterns and emplacement of the andesitic lava dome at Soufrière Hills Volcano, Montserrat, *in* Druitt, T.H., and Kokelaar, B.P., eds., The Eruption of Soufrière Hills Volcano, Montserrat, from 1995 to 1999: Geological Society London Memoirs, v. 21, p. 115–152, https://doi.org/10.1144/GSL.MEM.2002.021.01.06.

Wilson, L., and Head, J.W., 1994, Review and analysis of volcanic eruption theory and relationships to observed landforms: Reviews of Geophysics, v. 32, p. 221–263, https://doi.org/10.1029/94RG01113.

Witter, J.B., Kress, V.C., and Newhall, C.G., 2005, Volcán Popocatépetl, México. Petrology, magma mixing, and immediate sources of volatiles for the 1994-present eruption: Journal of Petrology, v. 46, p. 2337–2366, https://doi.org/10.1093/petrology/egi058.

Wright, R., Garbeil, H., and Harris, A.J.L., 2008, Using infrared satellite data to drive a thermo-rheological/stochastic lava flow emplacement model: A method for near-real-time volcanic hazard assessment: Geophysical Research Letters, v. 35, p. 1–5, https://doi.org/10.1029/2008GL035228.

Younger, Z.P., Valentine, G.A., and Gregg, T.K.P., 2019, 'A'ā lava emplacement and the significance of rafted pyroclastic material: Marcath volcano (Nevada, USA): Bulletin of Volcanology, v. 81, p. 1–50, https://doi.org/10.1007/s00445-019-1309-6.

Science Editor: Brad S. Singer
Associate Editor: Richard Waitt

Manuscript Received 30 April 2021
Revised Manuscript Received 28 September 2021
Manuscript Accepted 15 December 2021

Printed in the USA